JNeurosci
THE JOURNAL OF NEUROSCIENCE

Research Articles | Systems/Circuits

Phase-Structured Neuronal Recruitment in Motor Cortex during Skilled Movement Reorganized Early after Stroke

https://doi.org/10.1523/JNEUROSCI.0685-26.2026

Received: 25 April 2026
Revised: 4 October 2026
Accepted: 9 November 2026

Copyright © 2026 the authors

This Early Release article has been peer reviewed and accepted, but has not been through the composition and copyediting processes.The final version may differ slightly in style or formatting and will contain links to any extended data.

Alerts: Sign up at www.jneurosci.org/alerts to receive customized email alerts when the fully formatted version of this article is published.

Phase-Structured Neuronal Recruitment in Motor Cortex during Skilled Movement Reorganized Early after Stroke.

Di Chen[1,†], Yajun Zhou[2,†], Cheng'an Cao[3,4,†], Jin Gong[4], Qiyun Huang[5,6]
Jun Zhuang[7], Fang Jia[4], Ying Guo[4,*], and Yuanqing Li[1,6,*]

November 11, 2026

[1]School of Automation Science and Engineering, South China University of Technology, Guangzhou, China

[2]Department of Neurosurgery, Yale University, New Haven, CT, USA

[3]Department of Neurosurgery, Renmin Hospital of Wuhan University, Wuhan, China

[4]Department of Neurosurgery, The Third Affiliated Hospital of Sun Yat-sen University, Guangzhou, China

[5]School of Future Technology, South China University of Technology, Guangzhou, China

[6]Research Center for Brain–Computer Interface, Pazhou Laboratory, Guangzhou, China

[7]School of Information Engineering, Guangdong University of Technology, Guangzhou, China

[†]These authors contributed equally to this work.

[*]Corresponding authors: guoy@mail.sysu.edu.cn; auyqli@scut.edu.cn

Skilled forelimb movement engages both oscillatory and spiking activity in the motor cortex. However, how oscillatory phase organizes neuronal recruitment during behavior remains unclear. Here,

JNeurosci Accepted Manuscript

we performed longitudinal bilateral recordings of local field potentials and single-unit activity in the rat (male) caudal forelimb area during a single-pellet retrieval task before and after stroke. Stroke altered spectral organization and redistributed neuronal recruitment across hemispheres. In the CFA contralateral to the reaching forelimb, which was the lesioned hemisphere, firing rates decreased and spike timing became more variable, whereas spike-LFP phase consistency increased in low-frequency bands. In contrast, the CFA ipsilateral to the reaching forelimb showed increased firing and reduced low-frequency phase consistency. These results demonstrate that early post-stroke motor cortical reorganization does not simply weaken neural activity but reshapes neuronal recruitment into a phase-structured form within ongoing oscillatory activity, providing insight into the dynamical principles underlying motor cortical reorganization during skilled movement.
Keywords: skilled forelimb movement, motor cortex, oscillatory phase, spike-LFP phase, cortical stroke

Significance Statement

Skilled movement depends on coordinated interactions between population-level oscillations and neuronal spiking, but how this organization changes after cortical injury remains unclear. Using longitudinal bilateral recordings during skilled forelimb behavior, we show that early post-stroke reorganization is not characterized by a uniform loss of cortical activity. In the CFA contralateral to the reaching forelimb, firing was reduced and spike timing became more variable, yet low-frequency spike-LFP phase consistency increased. The ipsilateral CFA showed the opposite pattern, with increased firing and reduced low-frequency phase consistency. These findings demonstrate that firing output and spike–phase organization can reorganize independently after stroke, revealing a phase-structured dimension of motor cortical activity that is not captured by firing rate alone.

Introduction

Voluntary movement requires neural activity across multiple levels of organization, from oscillatory population dynamics in local

JNeurosci Accepted Manuscript

field potentials to the millisecond timing of neuronal spiking that supports movement execution (Nudo, 2006; Harrison et al., 2012; Yang et al., 2023). In the rodent, the caudal forelimb area (CFA) is the critical hub for skilled forelimb execution, analogous to the primate primary motor cortex (Touvykine et al., 2020; Brown and Teskey, 2014; Hira et al., 2013). While it is established that CFA activity drives movement, how oscillatory population activity relates to neuronal spiking during skilled forelimb movement remains unclear.

Movement-related activity in motor cortex is expressed in both low-frequency oscillations of local field potentials (LFPs) and spiking of neuronal ensembles. Low-frequency oscillations are consistently observed during movement preparation and execution and have been proposed to reflect population-level excitability states (Hall et al., 2014; Natraj et al., 2022; Ramanathan et al., 2018; Schalk et al., 2007; Khanna and Carmena, 2017; Choi et al., 2025; Saleh et al., 2010). In parallel, spiking activity in CFA carries movement-related information at the single-neuron and ensemble levels (Wang et al., 2023; Abbaspourazad et al., 2021; Bundy et al., 2019; Riehle et al., 2013). Together, these findings indicate that CFA contains both prominent oscillatory dynamics and spike-based representations relevant to motor control. However, direct evidence linking movement-related spiking to concurrent oscillatory population activity during skilled forelimb movement remains limited.

Skilled forelimb movements exhibit a strong contralateral bias at the cortical level relative to the moving limb (York, 2002) , and unilateral cortical lesions commonly lead to contralesional motor deficits (Duncan et al., 1992; Bashir et al., 2012). Accordingly, studies of skilled forelimb movement have primarily focused on the contralateral motor cortex (Wang et al., 2023; Abbaspourazad et al., 2021; Bundy et al., 2019; Riehle et al., 2013). However, movement-related activity is also observed in ipsilateral motor cortex during forelimb movements (Evarts, 1966; Tanji et al., 1987; Tanji et al., 1988; Aizawa et al., 1990; Bundy and Leuthardt, 2019). Despite this, ipsilateral CFA (iCFA) has been far less systematically examined in terms of its local oscillatory activity and ensemble spiking dynamics. Consequently, whether spiking is structured with respect to local oscillatory dynamics in a similar manner across contralateral CFA (cCFA) and iCFA remains largely unexplored.

At the cellular level, skilled forelimb movements are accompanied by recruitment of neurons in motor cortex (Hall et al., 2014;

JNeurosci Accepted Manuscript

Ramanathan et al., 2018; Ganguly et al., 2022; Arce-McShane et al., 2016; Elsayed et al., 2016). Such recruitment does not occur in isolation, but unfolds within ongoing oscillatory population dynamics that structure cortical activity over time (Bundy et al., 2019; Rule et al., 2015). This raises the possibility that oscillations provide a temporal framework for organizing ensemble spiking during movement. Whether neuronal recruitment exhibits systematic organization relative to oscillatory phase during skilled movement in either hemisphere remains to be determined.

To investigate this mechanism, we utilized transient middle cerebral artery occlusion (MCAO)-induced stroke not merely as a disease model, but as a pathophysiological perturbation to disrupt cortical dynamics (Longa et al., 1989; Rogers et al., 1997). Such perturbation provides an opportunity to examine motor cortical activity under a disrupted post-ischemic state, in which observed activity patterns may reflect both circuit-intrinsic properties and injury-related pathophysiological processes. Stroke is known to alter cortical excitability and population activity, potentially reshaping the organization of cortical dynamics (Ramanathan et al., 2018; Choi et al., 2025). Therefore, we hypothesized that skilled forelimb movements are associated with structured organization between ongoing oscillatory dynamics and neuronal spiking in CFA, including phase-dependent structure of spike timing, and that this organization differs between cCFA and iCFA following MCAO-induced stroke.

Here, we combined longitudinal electrophysiological recordings of LFPs and single-unit spiking in the CFA of rats performing a reach-and-grasp task before and early after stroke. By analyzing neuronal recruitment relative to ongoing oscillatory dynamics in both contralateral and ipsilateral hemispheres, we quantified changes in spike-LFP phase organization before and early after stroke, providing insight into how neuronal recruitment is reorganized within ongoing oscillatory activity in CFA.

Materials and Methods

Animals, care, and surgery

The subjects of this study were twelve healthy male Sprague-Dawley (SD) rats (9 weeks old at the time of stroke induction; body weight,

JNeurosci Accepted Manuscript

280–350 g).. Animals were obtained from Liaoning Changsheng Technology Company and housed in a specific pathogen-free (SPF) facility at the Experimental Animal Center of Guangzhou Shuiyuntian Biotechnology Company. The ambient temperature was maintained at 21 ± 2 °C under a 12 h light/12 h dark cycle. Rats had ad libitum access to water, while food intake was restricted during periods of task paradigm training.

All animal procedures were approved by the Animal Experimental Ethics Committee of the Third Affiliated Hospital of Sun Yat-sen University and the Academic Ethics Committee of Guangzhou Shuiyuntian Biotechnology Company (IACUC no. SYT2023110) and were conducted in accordance with established guidelines for animal care and use.

The overall experimental timeline is illustrated in Figure. 1A. Briefly, rats underwent SPR training during Weeks 0–1. Electrode implantation was performed in Week 2, followed by a postoperative recovery period. Pre-stroke baseline behavioral and electrophysiological recordings were collected in Week 3. Transient MCAO surgery was conducted in Week 4, and after a 7-day recovery period, early post-stroke behavioral and electrophysiological recordings were obtained in Week 5.

A total of 12 rats were initially included in the study. Following transient MCAO surgery, two rats were unable to perform the SPR task due to severe impairment of the right forelimb, and two rats died during the post-operative period. Consequently, behavioral and electrophysiological data from the remaining eight rats were included in the final analyses.

Behavioral training

Rats were trained on the single pellet retrieval (SPR) task, a widely used paradigm for assessing fine forelimb motor function (Schönfeld et al., 2017), using a custom-built automated training system. The automated SPR apparatus consisted of a behavioral chamber (40 cm × 30 cm × 25 cm) with a vertical slit (8 cm high, 1.2 cm wide) on the front wall. An automatic feeding device was positioned 0.5 cm in front of the chamber and controlled by a programmable microcontroller unit (MCU). Food pellets (Bio-Serv, Dustless Precision Pellets, 45 mg, Product No. F0023) were delivered by a robotic arm from the feeding compartment. Sensors installed at both ends of the feeding

JNeurosci Accepted Manuscript

device monitored pellet movement. During training, forelimb preference was assessed, and all rats exhibited a stable right forelimb preference during the SPR task. Therefore, the right forelimb was used for reaching in all behavioral and electrophysiological recordings.

For each trial, when a pellet appeared in the designated position, an auditory cue was presented and the front baffle of the chamber was opened, allowing the rat to initiate a reach-and-grasp movement. Removal of the pellet from the designated position triggered a transistor-transistor logic (TTL) signal generated by the feeding device sensors, which caused the baffle to close and the robotic arm to retract, preparing the system for the next trial. This closed-loop process enabled fully automated SPR training and precise behavioral event marking. The TTL signal was simultaneously sent to the electrophysiological recording system and used as a temporal marker for pellet retrieval events, which served as the alignment point for neural analyses (time = 0). Neural signals were recorded during SPR task performance.

Rats were trained on the SPR task for two weeks until stable performance was achieved, defined as a success rate exceeding 50%. Forelimb preference was monitored throughout the training period. During training and experimental sessions, food intake was mildly restricted to motivate task performance. Each rat received 30 pellets per day during training or testing sessions, with additional food provided after each daily session (see Supplementary Information for details). Body weight was monitored daily and maintained above 90% of the pre-training baseline. Water was available ad libitum, and rats were allowed unrestricted movement in their home cages outside training sessions.

Electrode implantation

Following SPR training (Weeks 0–1), recording electrodes were implanted in the bilateral CFA during Week 2. A custom microfilament electrode system comprising 16 channels in total was used, with one (2×4)-channel array implanted in each hemisphere. The two arrays were centered bilaterally in the caudal forelimb area at AP (+0.5) mm and ML (±3.0) mm relative to Bregma, corresponding to a 6-mm distance between the centers of the left and right arrays. Electrodes were fabricated from 35-μm nickel–titanium wires,

JNeurosci Accepted Manuscript

with impedances ranging from 100 to 200 kΩ.

Based on previous studies, the stereotaxic coordinates of the CFA center were defined as anteroposterior (AP) 0.5 mm and mediolateral (ML) 3.0 mm relative to bregma(Ramanathan et al., 2006). Rats were anesthetized with isoflurane and positioned in a stereotaxic apparatus. After aseptic preparation, a midline scalp incision was made to expose the skull. A rectangular craniotomy (3 mm × 2 mm) was created bilaterally, centered on the CFA coordinates. Additional holes were drilled in the frontal and occipital bones to secure screws for ground and reference connections.

The dura mater was carefully removed, and the microfilament array electrodes were implanted to a depth of 1550 ± 100 μm from the cortical surface(Isomura et al., 2009; Hooks et al., 2011), avoiding visible surface blood vessels (Figure. 1B). Electrodes were secured using dental cement, and body temperature was maintained throughout the surgical procedure. Penicillin was administered for three consecutive days postoperatively to prevent infection. Electrode placement was assessed postmortem in a subset of animals using HE-stained coronal sections; detailed procedures and representative electrode-track images are provided in the Supplementary Methods and Figure. S6.

Stroke model

Transient cerebral ischemia was induced during Week 4 using the intraluminal filament MCAO method as previously described by Longa et al.(Longa et al., 1989; Rogers et al., 1997). As all rats exhibited right forelimb preference, occlusion was performed in the left middle cerebral artery. Briefly, a silicone-coated filament was introduced through the external carotid artery and advanced via the internal carotid artery to the origin of the middle cerebral artery to induce cerebral blood flow occlusion. After 60 min of occlusion, the filament was withdrawn to allow reperfusion.

Neurological deficits were evaluated on the second day after surgery using the Longa scoring system. Rats with Longa scores between 1 and 3 were included in subsequent experiments. After a recovery period of a week (7 days), rats were re-evaluated using the SPR task, during which LFP and spike signals were recorded (Figure. 1A).

JNeurosci Accepted Manuscript

Histological assessment of electrode placement

Electrode placement was assessed postmortem in a subset of animals using HE-stained coronal sections. Electrode tracks were identified in relation to the intended bilateral caudal forelimb area (CFA) recording coordinates. The bilateral CFA arrays were targeted to AP +0.5 mm and ML ±3.0 mm relative to bregma, based on previous studies defining the CFA recording region (Ramanathan et al., 2006). Electrodes were implanted to a depth of 1550 ± 100 μm from the cortical surface, corresponding approximately to deep layers of motor cortex (Isomura et al., 2009; Hooks et al., 2011). Electrode-track locations in the examined animals were consistent with the intended bilateral CFA recording sites. Representative HE-stained sections showing electrode tracks are shown in Figure. S6.

Histological assessment of infarct location

Following the final electrophysiological recording session, animals were deeply anesthetized and euthanized for postmortem histological assessment. To verify infarct location after MCAO, brains from four rats were rapidly removed and processed for 2,3,5-triphenyltetrazolium chloride (TTC) staining (Longa et al., 1989; Rogers et al., 1997). Coronal brain sections were examined to identify ischemic tissue and to assess whether the infarct involved the targeted contralateral motor cortical region. In another subset of animals, brains were harvested after transcardial perfusion with phosphate-buffered saline (PBS) followed by paraformaldehyde, processed for frozen sectioning, and stained with hematoxylin and eosin (HE). HE-stained sections were used to further evaluate infarct location and tissue morphology. Across the examined animals, infarcts were observed in the targeted motor cortical region, with variability in lesion extent across animals. Representative TTC and HE images used for infarct verification are shown in Figure. S7.

Electrophysiological recordings

Raw neural signals were acquired using a 16-channel microfilament array electrode at a sampling rate of 30 kHz with the NeuroStudio electrophysiological acquisition system in combination with the NeuroLego system (Shanhai Medical Ltd., Nanjing, China). Local

JNeurosci Accepted Manuscript

field potentials (LFPs) and spike signals were amplified and digitized for subsequent processing. All recordings were performed inside a copper-mesh Faraday cage, with the acquisition system grounded to reduce external electrical interference.

After electrode implantation and a 7-day recovery period, pre-stroke baseline electrophysiological recordings were collected in Week 3 during both anesthetized resting conditions and SPR task performance. Transient MCAO surgery was performed in Week 4, followed by a 7-day recovery period. Early post-stroke behavioral and electrophysiological recordings were then obtained in Week 5 during SPR task performance.

Electrophysiology

Single-Unit Extraction

Spike data were sampled at 30 kHz and band-pass filtered offline between 300 and 3000 Hz using a zero-phase filter. For each animal and electrode, the pre- and early post-stroke recordings were concatenated and jointly spike-sorted using Tridesclous implemented in the SpikeInterface package (Buccino et al., 2020). This procedure maintained a common putative unit identity across recording sessions. The resulting spike trains were then separated according to their original pre- and early post-stroke recording periods, allowing paired comparisons of single-unit activity across conditions. Unit quality was assessed using refractory-period violations, total spike count, and manual inspection. Units were retained for analysis only if the inter-spike interval (ISI) violation fraction was below 10% and the total number of detected spikes exceeded 200. Additional spike-sorting quality metrics (coefficient of variation, waveform peak signal-to-noise ratio, waveform amplitude) are presented in Figure. S4. Electrode impedances remained below 300 kΩ after the early post-stroke recordings.

Local Field Potential

Local field potential (LFP) signals were acquired at a sampling rate of 1,000 Hz. Offline, the signals were bandpass filtered between 0.5 and 200 Hz and further processed using a 50 Hz notch filter to remove power-line interference. To mitigate channel-specific noise

JNeurosci Accepted Manuscript

and variability, signals from the eight electrodes within each hemisphere were averaged (see Figure. 1B), yielding one representative LFP time series per hemisphere for subsequent analyses.

Neural data analysis

LFP peak metric analysis

For each trial, LFP signals were segmented into a 3 s epoch (-1.5 to 1.5 s) aligned to the onset of pellet retrieval. Trial-wise LFP epochs were analyzed separately for pre-stroke and early post-stroke sessions within each hemisphere. For visualization only, condition-averaged LFP waveforms were obtained by averaging aligned trials within each hemisphere (Figure. 2A and 2C). In addition to the broadband LFP signal, band-limited signals were extracted using band-pass filters corresponding to five canonical frequency bands: delta (1–4 Hz), theta (4–8 Hz), alpha (8–13 Hz), beta (13–30 Hz), and gamma (30–100 Hz) (Buzsáki, 2006). Peak-related metrics were computed independently for each trial within the symmetric analysis window [-1.5, 1.5] s for both broadband and band-limited signals.

Peak Latency: For each trial, the Peak Latency was defined as the time point at which the LFP signal reached its maximum amplitude within the analysis window $[-1.5, 1.5]$ s,

$$t_{\text{peak}} = \arg \max_{t \in [-1.5, 1.5]} x(t), \tag{1}$$

where $x(t)$ denotes the trial-wise LFP waveforms.

Peak Value: For each trial, the Peak Value was defined as the maximum LFP amplitude within the same analysis window,

$$A_{\text{peak}} = \max_{t \in [-1.5, 1.5]} x(t), \tag{2}$$

following standard time-domain signal analysis conventions (Buzsáki, 2006).

Peak Height: To quantify peak prominence relative to surrounding activity, Peak Height was defined based on local troughs before and after the peak, following commonly used approaches in time-domain LFP and ERP analyses (Luck, 2014). Specifically, the pre-peak trough was defined as

$$A_{\text{trough}}^{\text{pre}} = \min_{t \in [-1.5,\, t_{\text{peak}}]} x(t), \tag{3}$$

JNeurosci Accepted Manuscript

and the post-peak trough was defined as

$$A_{\text{trough}}^{\text{post}} = \min_{t \in [t_{\text{peak}},\, 1.5]} x(t). \tag{4}$$

Peak Height was then computed as

$$H_{\text{peak}} = A_{\text{peak}} - \frac{A_{\text{trough}}^{\text{pre}} + A_{\text{trough}}^{\text{post}}}{2}, \tag{5}$$

providing a measure of peak prominence relative to the local baseline.

Response Recovery Time: Response recovery time quantified the latency from the peak amplitude to the sustained return of the signal to its baseline fluctuation range within the analysis window $[-1.5,\, 1.5]$ s relative to event onset ($t = 0$).

For each trial, the LFP signal $x(t)$ was baseline-corrected by subtracting the mean amplitude within a pre-event baseline window $\mathcal{W}_b = [t_{b1}, t_{b2}] \subset [-1.5, -1.3]$,

$$x_b(t) = x(t) - \frac{1}{|\mathcal{W}_b|} \int_{\mathcal{W}_b} x(\tau)\, d\tau. \tag{6}$$

To reduce high-frequency fluctuations, a moving-average filter of duration w was applied to obtain a trend signal

$$\tilde{x}_b(t) = \frac{1}{w} \int_{t-w/2}^{t+w/2} x_b(\tau)\, d\tau. \tag{7}$$

The temporal derivative of the trend signal was computed as

$$s(t) = \frac{d\tilde{x}_b(t)}{dt}. \tag{8}$$

Baseline-derived stability thresholds were defined from the baseline segment $t \in \mathcal{W}_b$. The slope threshold was defined as the q-th quantile of the absolute baseline slope,

$$\theta_s = Q_q\left(\{|s(t)| : t \in \mathcal{W}_b\}\right), \tag{9}$$

and the amplitude threshold was defined as

$$\theta_a = k\, \mathrm{SD}\left(\{\tilde{x}_b(t) : t \in \mathcal{W}_b\}\right), \tag{10}$$

where $\mathrm{SD}(\cdot)$ denotes the standard deviation and k is a scaling constant.

JNeurosci Accepted Manuscript

Let t_{peak} denote the peak latency defined previously. The response recovery time t_{rec} was defined as the first time point after the peak at which the signal returned to the baseline-defined range and remained within that range for at least D seconds. A time point t was considered stable when both the trend amplitude and its temporal derivative were within their respective baseline-derived thresholds, i.e.,

$$|\tilde{x}_b(t)| \leq \theta_a \quad \text{and} \quad |s(t)| \leq \theta_s. \tag{11}$$

Formally, t_{rec} was defined as the smallest $t > t_{\text{peak}}$ such that (Luck, 2014)

$$|\tilde{x}_b(\tau)| \leq \theta_a \quad \text{and} \quad |s(\tau)| \leq \theta_s, \quad \text{for all } \tau \in [t,\, t + D]. \tag{12}$$

If no sustained stable interval was detected, t_{rec} was defined as the post-peak time point minimizing the absolute trend amplitude,

$$t_{\text{rec}} = \arg\min_{t > t_{\text{peak}}} |\tilde{x}_b(t)|. \tag{13}$$

LFP aperiodic analysis

The aperiodic exponent of the power spectrum was analyzed to characterize excitation-inhibition balance inferred from LFP recordings (Gao et al., 2017). Power spectra were estimated on a trial-by-trial basis from hemisphere-averaged LFP signals using Welch's method (see Figure. 2E). For each trial, the power spectrum from 1 to 100 Hz was parameterized using the Python package *FOOOF* (Donoghue et al., 2020), which decomposes the spectrum into an aperiodic component and superimposed periodic peaks. Under the fixed aperiodic model, the aperiodic component was described by $\log_{10} P(f) = b - \chi \log_{10} f$, where b is the offset and χ is the aperiodic exponent. The aperiodic exponent was extracted for subsequent statistical analyses, and periodic peak parameters were used to identify trials containing detectable peaks within the canonical delta, theta, alpha, beta, and gamma frequency ranges.

Spike metric analysis

Spike-based metrics were computed on a trial-by-trial basis and summarized at the single-unit level. Spike times were segmented into trials using a 3 s window spanning from 1.5 s before to 1.5 s

JNeurosci Accepted Manuscript

after the task-related event (time zero), consistent with the LFP analyses. All metrics were calculated separately for each experimental condition (see Figure. 3E).

Mean firing rate: For each unit, the firing rate in trial i was computed as $r_i = N_i/3$ (Hz), where N_i is the number of spikes within the 3 s window (Zheng et al., 2022); the mean firing rate was then defined as $\bar{r} = \frac{1}{T}\sum_{i=1}^{T} r_i$ across trials.

Near-silent ratio: The near-silent ratio was calculated as the proportion of trials in which a unit emitted two or fewer spikes, providing a measure of sparse or suppressed firing activity across trials (Chen et al., 2008).

CV(ISI): Spike timing irregularity was quantified using the coefficient of variation of inter-spike intervals (CV(ISI)). For each trial containing at least 3 spikes, CV(ISI) was computed as the standard deviation of inter-spike intervals divided by their mean (i.e., $\mathrm{CV} = \sigma_{\mathrm{ISI}}/\mu_{\mathrm{ISI}}$, where σ_{ISI} and μ_{ISI} denote the standard deviation and mean of the inter-spike interval distribution within a trial, respectively) (Taube, 2010; Nawrot et al., 2008). Higher CV(ISI) means more irregular and less reliable spiking, while lower CV(ISI) means more regular and reliable neuronal firing. Trials with fewer than three spikes were excluded from CV(ISI) estimation. For each unit, CV(ISI) values were aggregated across eligible trials, and the median CV(ISI) was taken as the unit-level measure. The number of trials contributing to CV(ISI) estimation and the number of active trials (defined as trials containing more than two spikes) were recorded for quality control.

Fano factor: Trial-to-trial variability in spike counts was assessed using the Fano factor (Churchland et al., 2010). For each unit, spike counts were computed for individual trials within the 3 s analysis window. Only active trials containing more than 3 spike were included. The Fano factor was defined as

$$\text{Fano factor} = \frac{\sigma_N^2}{\mu_N}, \tag{14}$$

where σ_N^2 and μ_N denote the variance and mean of trial-wise spike counts, respectively. The Fano factor was calculated provided that at least eight active trials were available. Units not meeting this criterion were excluded from Fano factor analysis.

JNeurosci Accepted Manuscript

Grouping of single units by direction of firing change

To group units by the direction of early post-stroke firing change, we compared pre- and early post-stroke movement-related firing rates for each unit within each hemisphere. Significant temporal clusters of post–pre differences were identified using a cluster-based permutation test (see Statistical analysis). Units were then assigned based on the sign of the post–pre difference within the significant cluster (see Figure. 4A): increased-firing (positive), decreased-firing (negative), or no-change (no significant cluster).

Spike-LFP phase analysis

Spike-LFP phase extraction: Spike-LFP phase relationships were analyzed to characterize the temporal coupling between neuronal spiking activity and ongoing LFP oscillations (Voloh et al., 2020; Mizuseki et al., 2009). For each trial, LFP signals were band-pass filtered into five canonical frequency bands (delta, theta, alpha, beta, and gamma). The instantaneous phase of each band was extracted using the Hilbert transform (Le Van Quyen et al., 2001). Spike times were aligned to the corresponding instantaneous LFP phase values derived from the hemisphere-averaged LFP signal. Specifically, LFP signals were averaged across the eight electrodes within each hemisphere, and spikes from individual units were assigned to the corresponding hemispheric LFP based on the anatomical location of the recording channel (see Figure. 5).

For a given frequency band, the analytic signal of the LFP was computed as (Le Van Quyen et al., 2001):

$$z(t) = x(t) + i\,\mathcal{H}\{x(t)\}, \tag{15}$$

where $x(t)$ denotes the band-limited LFP signal and $\mathcal{H}\{\cdot\}$ represents the Hilbert transform. The instantaneous phase was then obtained as

$$\phi(t) = \arg(z(t)). \tag{16}$$

For each spike occurring at time t_k, the corresponding LFP phase $\phi_k = \phi(t_k)$ was assigned.

Trial-level spike-phase distribution: For each trial and frequency band, a spike-phase distribution was constructed from the set of phases

$$\{\phi_k\}_{k=1}^{N}, \tag{17}$$

JNeurosci Accepted Manuscript

where N is the number of spikes within the trial. Trials containing an insufficient number of spikes were excluded from subsequent phase analyses to ensure reliable estimation of phase distributions.

Pairwise Phase Consistency (PPC): Spike–LFP phase consistency was quantified using PPC, an unbiased measure of phase locking that is not systematically inflated by differences in the number of spike-phase observations across units or conditions (Vinck et al., 2010). For each unit and frequency band, PPC quantified the similarity of LFP phases sampled at individual spike times across trials.

For each pair of spike-associated phase observations, ϕ_i and ϕ_j, phase similarity was defined as the cosine of their circular phase difference:

$$\cos(\phi_i - \phi_j). \tag{18}$$

PPC was calculated as the mean phase similarity across all unique pairs of spike phases derived from different trials:

$$\mathrm{PPC} = \frac{1}{N_{\mathrm{pair}}} \sum_{i<j \ \mathrm{trial}(i)\neq\mathrm{trial}(j)} \cos(\phi_i - \phi_j), \tag{19}$$

where N_{pair} denotes the total number of valid cross-trial spike-phase pairs. Restricting the calculation to pairs of spikes from different trials reduced the potential influence of within-trial spike-train structure, including spike bursting and refractory effects, on the estimate of spike–LFP phase consistency (Vinck et al., 2010).PPC was calculated only for units with more than five spikes per trial and more than five trials before and after stroke. This criterion excluded extremely sparse observations for which phase-consistency estimates would be poorly constrained.

PPC values near zero indicate that spike-associated phases were broadly distributed across the oscillatory cycle, whereas positive PPC values indicate that spikes occurred at similar LFP phases across trials. Higher PPC values therefore reflect stronger and more consistent spike–LFP phase locking. PPC was calculated separately for each unit, frequency band, hemisphere, and recording session. Units with insufficient valid spike-phase observations or valid cross-trial phase pairs were excluded from PPC analyses.

Spike-count-matched PPC analysis

To assess whether differences in spike number associated with pre- and early post-stroke firing-rate changes influenced the PPC results,

JNeurosci Accepted Manuscript

we performed an additional spike-count-matched sensitivity analysis. For each unit, frequency band, and recording condition, trials containing at least five valid spike-associated phase observations were retained. Units were included when at least five such trials were available.

For each eligible trial, five spike-associated phases were randomly sampled without replacement, corresponding to the minimum spike-count criterion (≥ 5 spikes per trial) used in the original trial-wise PPC analysis. Trial-wise PPC was then calculated from these five spike-associated phases.

$$\mathrm{PPC}_{\mathrm{trial}} = \frac{\left|\sum_{k=1}^{N} e^{i\phi_k}\right|^2 - N}{N(N-1)}, \tag{20}$$

where $N = 5$ and ϕ_k denotes the LFP phase associated with the k-th sampled spike. Trial-wise PPC values were averaged across valid trials to obtain one PPC estimate for each resampling iteration.

Random spike subsampling was repeated 1,000 times using a fixed random seed. For each unit, the mean PPC across the 1,000 resampling iterations was used as the final spike-count-matched PPC estimate. The resampling iterations were used only to stabilize the estimate and were not treated as independent observations. The 2.5th and 97.5th percentiles of the resampling distribution were used to visualize resampling variability in Figure. 8.

Pre- and early post-stroke spike-count-matched PPC values were compared separately within each hemisphere and frequency band using two-sided Welch's t-tests. Benjamini–Hochberg false-discovery-rate correction was applied across the 10 hemisphere-by-frequency-band comparisons.

Quantification and statistical analysis

For all analyses, statistical significance was defined as $p < 0.05$. When multiple comparisons were involved, p-values were corrected using the Benjamini–Hochberg false discovery rate (FDR) procedure (Benjamini and Hochberg, 1995). Unless otherwise specified, statistical comparisons between pre-stroke and early post-stroke conditions were performed using linear mixed-effects models (Yu et al., 2022). In the spike metric analysis, pre- and early post-stroke conditions were compared within each hemisphere using linear mixed-effects

JNeurosci Accepted Manuscript

models, with condition included as a fixed effect and animal identity included as a random intercept. Time-resolved differences in population-averaged firing rate trajectories were assessed using cluster permutation tests performed separately in cCFA and iCFA (Maris and Oostenveld, 2007). In the spike-phase analysis, paired t-tests were performed at both the unit and animal levels.

Results

Experimental Framework and Movement-Related Neural Activity Before and Early After Stroke

To probe movement-related oscillatory activity and neuronal spiking during skilled forelimb behavior, rats were trained to perform a single-pellet retrieval (SPR) reach-and-grasp task (Figure. 1A) (Chen et al., 2014). The number of trials included in the analysis for each rat at both time points is provided in Table 1. After stable task performance was achieved, transient MCAO was induced to lesion the (cCFA) and perturb movement-related cortical activity (Figure. 1B). Neural activity, including LFPs and single-unit spiking, was recorded during task performance from chronically implanted microfilament arrays in both the cCFA (lesioned hemisphere) and (iCFA). In the present study, cCFA refers to the CFA contralateral to the reaching forelimb, whereas iCFA refers to the CFA ipsilateral to the reaching forelimb. All rats exhibited a right forelimb preference during the task. In the same animals, recordings were collected longitudinally one week before (pre-stroke) and one week after (early post-stroke) MCAO. At the early post-stroke time point, SPR success rates were significantly reduced compared with pre-stroke performance (pre-stroke: 0.621 ± 0.094; early post-stroke: 0.314 ± 0.111; paired t-test, $t(7) = 5.915$, $p < 0.001$, $n = 8$; Table S1). Using this framework, we compared movement-related oscillatory LFP dynamics and neuronal spiking before and early after stroke to quantify stroke-related changes in movement-related activity in each hemisphere (Figure. 1C and 1D). In all analyses, time 0 corresponds to pellet retrieval (pellet removal from the feeding device) during the skilled reach-and-grasp task. These movement-related signals provided the basis for subsequent analyses of how oscillatory dynamics structure spike timing before and early after stroke. Additional details regarding behavioral train-

JNeurosci Accepted Manuscript

ing, electrode implantation, stroke model, electrophysiological data acquisition and analysis are described in the Methods.

Preserved Peak Timing but Reorganized Response Evolution of Movement-Related LFPs Early After Stroke

To examine stroke-induced changes in movement-related population field responses, we first analyzed movement-related LFP waveforms (Figure. 2A and 2C) and quantified peak latency of the broadband LFP and band-limited signals in cCFA and iCFA. No significant differences in peak latency were observed between pre- and early post-stroke recordings for the raw LFP signal in either hemisphere (all $p > 0.05$; Figure. 2B and 2D, peak latency). Similarly, peak latency within delta, theta, alpha, beta, and gamma bands remained stable early after stroke in both hemispheres (all $p > 0.05$). Thus, the latency of the peak LFP response remained unchanged early after stroke.

In contrast to preserved peak timing, stroke significantly altered the dynamics of movement-related LFP responses. Quantification of peak metrics revealed significant changes in peak magnitude (value and height) across frequency bands following stroke (Figure. 2B and 2D, peak value and peak height). In addition, the response recovery time was significantly shortened in the broadband signal (cCFA: $\beta = -0.12$, $z = -3.36$, $p_{FDR} < 0.05$; iCFA: $\beta = -0.067$, $z = -4.59$, $p_{FDR} < 0.001$), indicating accelerated decay of the population response after the peak. These changes in peak magnitude (peak value and peak height) and response recovery time were frequency- and hemisphere-dependent: in the cCFA, significant pre-post differences in peak magnitude were detected in the delta, theta, and alpha bands (all $p < 0.05$), whereas beta- and gamma-band peak magnitude did not show detectable pre-post differences (all $p > 0.05$), and response recovery time was not significantly altered across frequency bands ($p > 0.05$); in the iCFA, significant pre-post differences in peak magnitude were observed across multiple frequency bands (all $p < 0.05$).

Beyond the time-domain response dynamics, we next examined whether the broader spectral organization of motor cortical activity was altered early after stroke. Power spectral density (PSD) analyses revealed a marked early post-stroke increase in the aperiodic exponent in both cCFA and iCFA (cCFA: $\beta = 0.268$, $z = 9.83$,

JNeurosci Accepted Manuscript

$p < 0.001$; iCFA: $\beta = 0.119$, $z = 4.35$, $p_{FDR} < 0.001$; Figure. 2E, Figure. S1 and Figure. S2), indicating reorganization of the baseline spectral structure of population field activity. Time-frequency representations further revealed that, following stroke, spectral power was redistributed over time, with increased low-frequency (4–10 Hz) activity during the post-movement period in both hemispheres (Figure. 2F). Direct comparison of post-pre differences identified significant clusters of modulation primarily within the 4–10 Hz range in the ipsilateral CFA, with the most prominent changes occurring before pellet retrieval, as confirmed by cluster-based permutation tests (Figure. 2G). No consistent modulation was observed in higher frequency ranges (30–100 Hz; see Figure. S3)

Together, these results reveal a dissociation in field-level dynamics following stroke: the timing of the dominant LFP peak remained stable, whereas the recovery dynamics, baseline spectral structure, and time-resolved spectral organization of population field activity were substantially reorganized in a hemisphere- and frequency-dependent manner.

Asymmetric Reorganization of Neuronal Recruitment and Spike Reliability Early After Stroke

We first visualized movement-related single-unit activity using z-scored peri-event firing rates (PETH) heatmaps in the cCFA and iCFA (Figure. 3A and 3B). Following stroke, cCFA units exhibited markedly reduced movement-related recruitment, whereas ipsilateral units showed an apparent enhancement of movement-related activity at the pooled-unit level. These opposing patterns were also evident in the pooled population firing-rate envelopes, which showed decreased cCFA output and increased ipsilateral firing early after stroke (Figure. 3C and 3D). These effects were confirmed by separate cluster permutation tests in cCFA and iCFA, each revealing a significant temporal cluster spanning the entire analyzed time window ($p < 0.05$; see Methods). To address the hierarchical structure of the recordings, we additionally performed animal-level analyses in which each metric was first summarized across units within each animal and hemisphere, followed by paired pre–post comparisons across animals ($n = 8$). Unit-level analyses are shown to characterize the distribution and direction of single-unit changes, whereas animal-level analyses were used to assess whether the prin-

JNeurosci Accepted Manuscript

cipal effects were consistently expressed across animals.

Consistent with the population-level pattern, both unit-level and animal-level analyses indicated reduced contralateral neuronal recruitment early after stroke. At the animal level, mean firing rate in the cCFA decreased significantly early after stroke (pre: 22.48 Hz; post: 6.88 Hz; paired t-test, $t(7) = 2.60$, $p = 0.035$), with decreases observed in seven of eight animals (Figure. 3E). At the unit level, this reduction was accompanied by an increased near-silent ratio; however, the near-silent-ratio change was not significant at the animal level ($p = 0.140$). In the iCFA, pooled-unit analyses showed increased firing rates together with reduced near-silent ratios early after stroke (Figure. 3F). However, neither effect was significant at the animal level (mean firing rate: $p = 0.203$; near-silent ratio: $p = 0.494$), indicating that these ipsilateral recruitment patterns were not consistently expressed across animals.

We next assessed whether the contralateral reduction in neuronal recruitment was accompanied by altered spike reliability. Within-trial spike-timing irregularity and trial-to-trial firing variability were quantified using CV(ISI) and Fano factor, respectively (see Methods). In the cCFA, animal-level analyses confirmed significant increases in both metrics early after stroke. CV(ISI) increased from 1.25 to 2.03 ($t(7) = -4.86$, $p = 0.0018$), with increases observed in all eight animals, and the Fano factor increased from 7.12 to 10.45 ($t(7) = -3.92$, $p = 0.0058$), also increasing in all eight animals (Figure. 3E). These findings indicate elevated within-trial spike-timing irregularity and greater trial-to-trial firing variability in the cCFA early after stroke. In contrast, neither CV(ISI) nor Fano factor changed significantly in the iCFA at the animal level (CV[ISI]: $p = 0.939$; Fano factor: $p = 0.137$; Figure. 3F). To further characterize relationships among contralateral neuronal features, we performed exploratory unit-level analyses of post–pre differences (Δ) across metrics (Figure. 3G). ΔCV(ISI) and ΔFano factor were strongly correlated across units (Pearson $r = 0.65$, $p = 0.00016$). Changes in the near-silent ratio were negatively correlated with ΔCV(ISI) ($r = -0.49$, $p = 0.0075$), but were not significantly associated with ΔFano factor ($r = -0.32$, $p = 0.096$).

Together, these results demonstrate robust contralateral reorganization of spiking early after stroke, characterized by reduced mean firing rate, increased spike-timing irregularity, and increased trial-to-trial firing variability across animals. Although pooled-unit anal-

JNeurosci Accepted Manuscript

yses suggested increased ipsilateral recruitment, this pattern was not consistently preserved at the animal level, and ipsilateral spike reliability remained unchanged.

Single-Unit Subpopulations with Increased or Decreased Firing Early After Stroke

The population-level firing rate envelopes above showed reduced contralateral output and increased ipsilateral firing early after stroke (Figure. 3C and 3D). To characterize these changes at the level of individual units over time, pre- and early post-stroke movement-related firing rate trajectories were compared for each unit, and significant temporal clusters were identified using a cluster permutation test (Fig4A; see Methods).

Significant temporal clusters were identified for each unit when detected, and units were classified within each hemisphere according to the direction of the post–pre difference within the significant cluster as increased-firing or decreased-firing; units without a significant cluster were labeled as no-change (Figure. 4B). The distribution of increased- and decreased-firing units differed between hemispheres. In cCFA, the majority of units were classified as decreased-firing (25/29), with only a small fraction showing increased firing (2/29) or no change (2/29). In iCFA, units were predominantly classified as increased-firing (30/45), with fewer units showing decreased firing (10/45) or no change (5/45) (Figure. 4B).

Representative examples from each category illustrate the corresponding movement-related spiking patterns, with significant windows marked on the firing rate traces (Figure. 4A). As decreased-firing units predominated in the cCFA and increased-firing units predominated in the iCFA, subsequent analyses focused on these subpopulations.

Reorganization of Spike–LFP Phase Consistency Early After Stroke

We next quantified the consistency of spike timing relative to ongoing LFP phase across canonical frequency bands using pairwise phase consistency (PPC). PPC measures the extent to which spikes occurred at similar phases of the local oscillation across trials, with higher values indicating stronger and more reliable spike–LFP phase

JNeurosci Accepted Manuscript

locking (see Methods; Figure. 5A).

In the cCFA, PPC was significantly increased early after stroke in the delta, theta, alpha, and beta frequency ranges (delta: $t = -6.38$, $p_{\text{FDR}} < 0.001$; theta: $t = -8.64$, $p_{\text{FDR}} < 0.001$; alpha: $t = -6.33$, $p_{\text{FDR}} < 0.001$; beta: $t = -3.22$, $p_{\text{FDR}} < 0.01$; Figure. 5B). The largest early post-stroke increases were observed in the delta and theta bands, in which mean PPC increased from 0.054 to 0.220 and from 0.020 to 0.222, respectively. In contrast, gamma-band PPC did not differ between pre- and early post-stroke recordings ($p_{\text{FDR}} > 0.05$). The increase in contralateral PPC was further evident in the distributions of unit-level PPC values, which shifted toward higher values early after stroke in the frequency bands showing significant effects (Figure. 5B). Thus, early post-stroke contralateral units exhibited more consistent spike timing relative to the phase of low-frequency LFP oscillations across trials.

In contrast, the iCFA exhibited reduced PPC early after stroke in the delta, theta, and alpha bands (delta: $t = 3.32$, $p_{\text{FDR}} < 0.01$; theta: $t = 3.29$, $p_{\text{FDR}} < 0.01$; alpha: $t = 3.06$, $p_{\text{FDR}} < 0.01$; Figure. 5C). Mean PPC in these bands decreased toward zero early after stroke, indicating weaker cross-trial consistency of spike timing relative to the local LFP phase. No significant pre- to early post-stroke differences were observed in the ipsilateral beta or gamma bands ($p_{\text{FDR}} > 0.05$).

Complementary animal-level analyses confirmed the opposing hemispheric changes in low-frequency phase consistency. Contralateral PPC increased early after stroke in the delta, theta, and alpha bands ($N = 8$, all $p_{\text{FDR}} < 0.05$), whereas ipsilateral PPC decreased in the same frequency bands ($N = 5$, all $p_{\text{FDR}} < 0.05$). Beta- and gamma-band changes were not significant in either hemisphere. The smaller ipsilateral sample reflects the requirement for valid paired pre- and early post-stroke PPC estimates after application of the predefined trial- and unit-level inclusion criteria (Supplementary Table. S2). To assess whether these PPC changes were influenced by alterations in aperiodic spectral activity, we performed trial-wise spectral parameterization and repeated the PPC analysis using only trials with identifiable periodic peaks. The main hemispheric patterns were largely preserved, with increased PPC in the cCFA across delta, theta, alpha, and beta bands and decreased PPC in the iCFA in delta and theta bands (Figure. S5). Together, these analyses reveal a bidirectional reorganization of spike-LFP phase consistency

JNeurosci Accepted Manuscript

early after stroke: phase locking was strengthened in the cCFA, particularly in low-frequency bands, whereas phase consistency was reduced in the iCFA across the delta, theta, and alpha bands.

Effects of Pellet-Grasp Outcome on Early Post-Stroke Neural Activity

To determine whether pellet-grasp outcome influenced the observed early post-stroke changes, trials were separated according to whether the pellet was successfully grasped. All included trials contained the reach, grasp attempt, and forelimb retrieval sequence; therefore, unsuccessful trials referred to unsuccessful pellet grasping rather than unsuccessful reaching.

For successful pellet-grasp trials, the mean firing rate significantly decreased early after stroke in the cCFA ($t = 5.422$, $p < 0.001$), with 82.8% of units showing a decrease. In contrast, the firing rate significantly increased in the iCFA ($t = -3.640$, $p < 0.001$), with 73.9% of units showing an increase. A similar pattern was observed for unsuccessful pellet-grasp trials. The firing rate decreased in the cCFA ($t = 5.345$, $p < 0.001$), with 79.3% of units showing a decrease, and increased in the ipsilateral CFA ($t = -3.525$, $p < 0.001$), with 76.1% of units showing an increase (Figure. 6 A–B).

For successful pellet-grasp trials, PPC significantly increased early after stroke in the cCFA in the delta, theta, alpha, and beta bands following FDR correction. In the ipsilateral CFA, PPC significantly decreased in the delta, theta, and alpha bands, whereas no significant changes were observed in the beta or gamma bands. For unsuccessful pellet-grasp trials, PPC showed a generally similar directional pattern, with higher early post-stroke PPC in the cCFA and lower early post-stroke PPC in the ipsilateral CFA across most frequency bands. However, none of these differences remained significant after FDR correction, likely reflecting the smaller number of units available for the unsuccessful-trial analysis, particularly in the early post-stroke cCFA (Figure. 6 C–D).

Overall, separating trials according to pellet-grasp outcome did not alter the main directional pattern of the firing-rate and PPC changes observed early after stroke.

JNeurosci Accepted Manuscript

Spike–LFP Phase Consistency Across the Full Unit Population

To determine whether the PPC changes extended beyond the firing-rate-defined subpopulations, we repeated the analysis using all eligible units in the contralateral and ipsilateral CFA. In the contralateral CFA, PPC increased significantly after stroke in the delta ($t = -5.81$, $p_{\mathrm{FDR}} < 0.001$), theta ($t = -6.72$, $p_{\mathrm{FDR}} < 0.001$), alpha ($t = -5.65$, $p_{\mathrm{FDR}} < 0.001$), and beta bands ($t = -3.24$, $p_{\mathrm{FDR}} < 0.01$), whereas no significant change was observed in the gamma band ($t = 1.27$, $p_{\mathrm{FDR}} > 0.05$; Figure. S7A).

In the ipsilateral CFA, PPC decreased significantly after stroke in the delta ($t = 2.52$, $p_{\mathrm{FDR}} < 0.05$), alpha ($t = 2.54$, $p_{\mathrm{FDR}} < 0.05$), and beta bands ($t = 2.20$, $p_{\mathrm{FDR}} < 0.05$). The decrease in theta-band PPC did not remain significant after FDR correction ($t = 1.98$, $p_{\mathrm{FDR}} > 0.05$), and no significant change was observed in the gamma band ($t = 1.40$, $p_{\mathrm{FDR}} > 0.05$; Figure. 7B).

Together, the full-unit analysis revealed increased spike-LFP phase consistency across the delta-to-beta range in the contralateral CFA and reduced phase consistency in selected low-frequency bands in the ipsilateral CFA, consistent with a hemisphere-specific reorganization of spike timing relative to local oscillatory phase after stroke.

Spike-count-matched PPC analysis

The opposing hemispheric PPC changes were preserved after explicitly matching the number of spikes contributing from each trial (Figure. 8). In the cCFA, spike-count-matched PPC remained significantly increased after stroke in the delta, theta, and alpha bands (all $p_{\mathrm{FDR}} < 0.001$) and in the beta band ($p_{\mathrm{FDR}} < 0.01$), whereas no significant difference was observed in the gamma band.

In the iCFA, spike-count-matched PPC remained significantly reduced after stroke in the delta, theta, and alpha bands (all $p_{\mathrm{FDR}} < 0.01$). No significant pre–post differences were observed in the beta or gamma bands.

Thus, fixing the number of sampled spikes to five spikes per valid trial reproduced the principal bilateral low-frequency PPC pattern observed in the primary analysis. These results indicate that the increased cCFA PPC and decreased iCFA PPC were not simply consequences of differences in the number of spikes available for

JNeurosci Accepted Manuscript

phase-consistency estimation following the stroke-related changes in firing rate.

Discussion

Motor cortex generates skilled forelimb movements through population dynamics and precisely timed neuronal spiking (Churchland et al., 2012; Gallego et al., 2017; Kargo and Nitz, 2004). Low-frequency oscillatory activity is consistently observed during movement and is thought to participate in population-level activity(Hall et al., 2014; Natraj et al., 2022; Ramanathan et al., 2018; Schalk et al., 2007). However, whether spike timing is systematically organized within ongoing oscillatory dynamics during skilled movement has remained unclear. Here, using stroke as a pathophysiological perturbation of motor cortical dynamics, we examined how spike timing is organized relative to local oscillation phase during skilled movement. We found that spike timing exhibited structured alignment to low-frequency phase and that this phase-dependent organization was altered most strongly in the contralateral cortex, despite reduced firing output and degraded spike reliability. Importantly, these findings suggest that changes in spike-phase organization cannot be inferred from firing output alone. This combination provides a framework for interpreting the main findings: early post-stroke motor cortical activity was not simply reduced in magnitude, but exhibited stronger phase-dependent spike timing relative to ongoing low-frequency oscillatory activity. These findings indicate that early post-stroke changes in firing output and spike–phase organization can occur in different directions within motor cortex.

Stability of Peak Time and Alteration of Evolution in Response

Motor cortical LFP activity during skilled forelimb movement appears to exhibit temporally structured dynamics. In rodent reach-and-grasp paradigm, low-frequency field activity evolves across trials (Hall et al., 2014), and movement-related neural dynamics display reproducible temporal progression (Ramanathan et al., 2015). Using stroke as a perturbation of related motor cortical dynamics, we found that distinct temporal features of the dominant LFP response were differentially affected. Specifically, the peak timing

JNeurosci Accepted Manuscript

remained stable, whereas the subsequent recovery dynamics were altered (Figure. 2B and 2D). This differential effect suggests that the temporal position of the response peak and response evolution may reflect partially distinct temporal processes within motor cortical field activity. The greater sensitivity of waveform evolution to perturbation suggests that it may rely more heavily on local cortical circuitry than event-aligned peak position, providing new insight into how motor cortex organizes movement-related temporal structure.

Aperiodic Spectral Background Shifts Early After Stroke

We observed a significant increase in the aperiodic exponent of the LFP power spectrum early after stroke in both cCFA and iCFA, estimated over the 1–100 Hz range (Figure. 2E). The aperiodic component captures broadband spectral organization beyond narrowband oscillatory peaks (Donoghue et al., 2020). An increased aperiodic exponent reflects relatively increased low-frequency power and reduced high-frequency contributions across this range, indicating a redistribution of background spectral power following injury.

Although the present study does not directly measure synaptic excitation or inhibition, computational modeling has demonstrated that the aperiodic exponent is sensitive to excitation-inhibition (E/I) balance, with increased aperiodic exponents associated with reduced E/I ratios (Gao et al., 2017). Independent experimental work in rodent stroke models has reported increased $GABA_A$-mediated tonic inhibition and altered cortical excitability in peri-infarct motor cortex (Clarkson et al., 2010; Jaenisch et al., 2016). The bilateral steepening observed here is consistent with prior evidence that stroke alters cortical excitability, and indicates that broadband spectral structure is sensitive to stroke-related physiological changes in both hemispheres.

Stroke Differentially Alters Recruitment Strength and Reliability across Hemispheres

Skilled forelimb movement is cortically biased toward the contralateral hemisphere (York, 2002), which was directly targeted by the infarct in our model. In the lesioned cCFA, reduced firing rates and increased near-silent ratios, together with elevated CV(ISI) and

JNeurosci Accepted Manuscript

Fano factor, indicate that injury disrupts both recruitment strength and the stability with which neurons are reliably recruited into movement-related ensembles (Figure. 3E).

Previous fMRI and EEG studies have shown increased ipsilateral motor cortex activation during movement after unilateral stroke (Murase et al., 2004; Saikaley et al., 2022; Grefkes and Fink, 2014). Consistent with this observation, the iCFA exhibited increased firing rates without increased CV(ISI) or Fano factor (Figure. 3F), extending macroscopic observations of ipsilateral motor cortical activation to the level of single-unit dynamics. Together, these findings reveal hemispheric differences in recruitment strength and reliability early after stroke.

Bidirectional Reorganization of Spike–LFP Phase Consistency Early After Stroke

Spike–LFP phase consistency changed in opposite directions across hemispheres early after stroke. In the cCFA, increased low-frequency PPC accompanied reduced firing rates and greater spike variability, whereas the iCFA exhibited increased firing rates but reduced phase consistency (Figure. 5B,C). This dissociation suggests that spike–phase organization is not simply determined by firing output.

Oscillation phase has been proposed to reflect cyclical fluctuations in neuronal excitability that bias spike probability (Haegens et al., 2011; VanRullen, 2016; Buzsáki and Wang, 2012). The increased contralateral PPC suggests that spikes became more consistently aligned with ongoing low-frequency oscillations during skilled movement. Although these observations do not establish a causal role for phase organization in movement execution, they indicate that firing output and spike–phase consistency can change in different directions.

Previous studies have established low-frequency cortical dynamics as an important temporal framework for skilled motor behavior: reach-related low-frequency activity and spike–field coordination are disrupted after stroke and evolve during behavioral recovery (Ramanathan et al., 2018), low-frequency spike–LFP organization emerges with skilled reach learning (Fleischer et al., 2023), and low-frequency modulation can enhance task-related ensemble co-firing and motor performance after stroke (Khanna et al., 2021).

Building on this framework, our findings demonstrate a hemisphere-dependent reorganization of the relationship between neuronal re-

JNeurosci Accepted Manuscript

cruitment and ongoing low-frequency phase. Specifically, reduced and more variable firing in the cCFA was accompanied by increased phase consistency, whereas increased recruitment in the iCFA coincided with reduced phase consistency. This bilateral divergence suggests that early post-stroke reorganization involves distinct changes in recruitment strength and spike–phase organization across hemispheres.

Limitations of the Study

This study characterizes how stroke reshapes oscillation-spike organization within CFA, but several limitations should be noted. First, recordings were restricted to the contralateral and iCFA. Consequently, our analyses capture local dynamical reorganization but do not address interactions across the broader motor network. Motor recovery early after stroke involves distributed changes across premotor, parietal, and subcortical circuits, with inter-areal connectivity contributing to functional outcomes (Ward et al., 2003; Rehme and Grefkes, 2013; Grefkes and Ward, 2014; Dancause and Nudo, 2011). How the local oscillation-spike reorganization described here interacts with large-scale network dynamics therefore remains unclear.

A second limitation is the absence of cell-type identification. Because excitatory and inhibitory neurons may contribute differently to spike timing and oscillatory dynamics (Isaacson and Scanziani, 2011; Cardin, 2018), extracellular recordings alone cannot determine their respective contributions to the observed reorganization. Future cell-type-specific recordings will be needed to clarify the underlying mechanisms.

A third limitation concerns the behavioral resolution of the analysis. Skilled reaching involves multiple sensorimotor processes, including reaching, grasping, forelimb retrieval, and sensory feedback, which may engage partially distinct neural dynamics (Peters et al., 2014; Li et al., 2017). Although successful and unsuccessful pellet-grasp trials were analyzed separately, neural activity was aligned to pellet retrieval rather than to the onset of individual movement components. The main hemispheric pattern of spiking activity was preserved across successful and unsuccessful trials, suggesting that the observed reorganization was not restricted to a single behavioral outcome. This alignment provided a common reference point for characterizing neural activity during the SPR task but did not al-

JNeurosci Accepted Manuscript

low the contributions of individual movement components or paw kinematics to be distinguished. Future studies incorporating synchronized behavioral tracking and identification of specific movement events will help clarify how oscillatory organization and spike recruitment relate to paw trajectory, different components of skilled movement, and motor recovery early after stroke.

A fourth consideration is that the present study focused on neural activity during the SPR task. Although non-task activity was considered in the initial experimental design, freely moving animals exhibited a range of spontaneous behaviors, including locomotion, grooming, face washing, chewing, and postural movements (Mimica et al., 2023). In addition, the period before task performance was frequently affected by chewing-related noise. These factors made it difficult to define a comparable non-task period across trials and animals. Future studies incorporating a controlled non-task condition will help determine whether the observed changes are specific to skilled movement or also reflect broader alterations in cortical dynamics early after stroke.

Another limitation is that electrophysiological recordings were obtained at only one early post-stroke time point. Although SPR success rate provided a concurrent measure of skilled forelimb performance, the present design did not allow us to determine whether the magnitude of cortical reorganization scales with the severity of motor impairment or predicts subsequent recovery. Future studies combining repeated neural recordings with longitudinal neurological and task-specific behavioral assessments will be required to establish these relationships.

Finally, the absence of a sham-surgery control limits the interpretation of the bilateral 1/f slope steepening. Although this change may reflect stroke-related alterations in cortical activity, time-dependent effects of chronic electrode implantation, including gliosis or changes in the electrode–tissue interface, cannot be excluded. Future studies including sham-operated animals recorded over the same time interval will be needed to distinguish these effects.

Conclusions

In summary, our findings demonstrate that oscillatory population dynamics structure neuronal recruitment during skilled forelimb movement in motor cortex. Following cortical stroke, neuronal

JNeurosci Accepted Manuscript

recruitment and its phase-related organization were differentially altered across hemispheres. In the contralateral cortex, reduced firing output and increased spike variability coexisted with increased low-frequency spike–LFP phase consistency, whereas the ipsilateral cortex showed increased firing and reduced low-frequency phase consistency. These results indicate that neuronal recruitment during skilled movement can be reorganized in ways that differentially affect firing properties and phase-structured activity within ongoing oscillatory dynamics.

JNeurosci Accepted Manuscript

Supplementary information

Supplementary Results
Supplementary Methods
Figure. S1 and its legend in a PDF
Figure. S2 and its legend in a PDF
Figure. S3 and its legend in a PDF
Figure. S4 and its legend in a PDF
Figure. S5 and its legend in a PDF
Figure. S6 and its legend in a PDF
Figure. S7 and its legend in a PDF

Acknowledgements

This work was supported by the Brain Science and Brain-like Intelligence Technology-National Science and Technology Major Project (2022ZD0208900) and the National Natural Science Foundation of China (U22A20293, 62306120).

Declarations

The authors declare no competing interests.

Author contributions

Conceptualization, Yuanqing Li and Ying Guo; methodology, Di Chen; Formal analysis, Di Chen; investigation, Cheng'an Cao, Jin Gong and Fang Jia; writing original draft, Di Chen and Yajun Zhou; writing review & editing, Di Chen, Yajun Zhou, Qiyun Huang and Jun Zhang; funding acquisition, Yuanqing Li; resources, Ying Guo; supervision, Yuanqing Li and Ying Guo.

Resource availability

Lead contact

Requests for further information and resources should be directed to and will be fulfilled by the lead contact, Di Chen (dididichen@outlook.com).

JNeurosci Accepted Manuscript

Materials availability

This study did not generate new, unique reagents.

Data and code availability

The data and custom code that support the findings from this study are available from the lead contact upon reasonable request.

References

Abbaspourazad H, Choudhury M, Wong YT, Pesaran B, Shanechi MM (2021) Multiscale low-dimensional motor cortical state dynamics predict naturalistic reach-and-grasp behavior. *Nature communications* 12:607.

Aizawa H, Mushiake H, Inase M, Tanji J (1990) An output zone of the monkey primary motor cortex specialized for bilateral hand movement. *Experimental Brain Research* 82:219–221.

Arce-McShane FI, Ross CF, Takahashi K, Sessle BJ, Hatsopoulos NG (2016) Primary motor and sensory cortical areas communicate via spatiotemporally coordinated networks at multiple frequencies. *Proceedings of the National Academy of Sciences* 113:5083–5088.

Bashir S, Kaeser M, Wyss A, Hamadjida A, Liu Y, Bloch J, Brunet JF, Belhaj-Saif A, Rouiller EM (2012) Short-term effects of unilateral lesion of the primary motor cortex (m1) on ipsilesional hand dexterity in adult macaque monkeys. *Brain Structure and Function* 217:63–79.

Benjamini Y, Hochberg Y (1995) Controlling the false discovery rate: a practical and powerful approach to multiple testing. *Journal of the Royal statistical society: series B (Methodological)* 57:289–300.

Brown AR, Teskey GC (2014) Motor cortex is functionally organized as a set of spatially distinct representations for complex movements. *Journal of Neuroscience* 34:13574–13585.

Buccino AP, Hurwitz CL, Garcia S, Magland J, Siegle JH, Hurwitz R, Hennig MH (2020) Spikeinterface, a unified framework for spike sorting. *Elife* 9:e61834.

JNeurosci Accepted Manuscript

Bundy DT, Guggenmos DJ, Murphy MD, Nudo RJ (2019) Chronic stability of single-channel neurophysiological correlates of gross and fine reaching movements in the rat. *PloS one* 14:e0219034.

Bundy DT, Leuthardt EC (2019) The cortical physiology of ipsilateral limb movements. *Trends in neurosciences* 42:825–839.

Buzsáki G (2006) *Rhythms of the Brain* Oxford university press.

Buzsáki G, Wang XJ (2012) Mechanisms of gamma oscillations. *Annual review of neuroscience* 35:203–225.

Cardin JA (2018) Inhibitory interneurons regulate temporal precision and correlations in cortical circuits. *Trends in neurosciences* 41:689–700.

Chen CC, Gilmore A, Zuo Y (2014) Study motor skill learning by single-pellet reaching tasks in mice. *Journal of visualized experiments: JoVE* p. 51238.

Chen Y, Marchenko V, Rogers RF (2008) Sparse firing frequency-based neuron spike train classification. *Neuroscience letters* 439:47–51.

Choi H, Kim J, Khanna P, Griffin S, Novik L, Morecraft RJ, Morrison JH, Ganguly K (2025) Restoration of temporal separability between beta and movement ensemble co-firing with motor recovery. *Neuron* 113:4263–4277.

Churchland MM, Cunningham JP, Kaufman MT, Foster JD, Nuyujukian P, Ryu SI, Shenoy KV (2012) Neural population dynamics during reaching. *Nature* 487:51–56.

Churchland MM, Yu BM, Cunningham JP, Sugrue LP, Cohen MR, Corrado GS, Newsome WT, Clark AM, Hosseini P, Scott BB et al. (2010) Stimulus onset quenches neural variability: a widespread cortical phenomenon. *Nature neuroscience* 13:369–378.

Clarkson AN, Huang BS, MacIsaac SE, Mody I, Carmichael ST (2010) Reducing excessive gaba-mediated tonic inhibition promotes functional recovery after stroke. *Nature* 468:305–309.

Dancause N, Nudo RJ (2011) Shaping plasticity to enhance recovery after injury. *Progress in brain research* 192:273–295.

Donoghue T, Haller M, Peterson EJ, Varma P, Sebastian P, Gao R, Noto T, Lara AH, Wallis JD, Knight RT et al. (2020) Parameterizing neural power spectra into periodic and aperiodic components. *Nature neuroscience* 23:1655–1665.

JNeurosci Accepted Manuscript

Duncan PW, Goldstein LB, Matchar D, Divine GW, Feussner J (1992) Measurement of motor recovery after stroke. outcome assessment and sample size requirements. *Stroke* 23:1084–1089.

Elsayed GF, Lara AH, Kaufman MT, Churchland MM, Cunningham JP (2016) Reorganization between preparatory and movement population responses in motor cortex. *Nature communications* 7:13239.

Evarts EV (1966) Pyramidal tract activity associated with a conditioned hand movement in the monkey. *Journal of neurophysiology* 29:1011–1027.

Fleischer P, Abbasi A, Fealy AW, Danielsen NP, Sandhu R, Raj PR, Gulati T (2023) Emergent low-frequency activity in cortico-cerebellar networks with motor skill learning. *Eneuro* 10:ENEURO–0011.

Gallego JA, Perich MG, Miller LE, Solla SA (2017) Neural manifolds for the control of movement. *Neuron* 94:978–984.

Ganguly K, Khanna P, Morecraft RJ, Lin DJ (2022) Modulation of neural co-firing to enhance network transmission and improve motor function after stroke. *Neuron* 110:2363–2385.

Gao R, Peterson EJ, Voytek B (2017) Inferring synaptic excitation/inhibition balance from field potentials. *Neuroimage* 158:70–78.

Grefkes C, Fink GR (2014) Connectivity-based approaches in stroke and recovery of function. *The Lancet Neurology* 13:206–216.

Grefkes C, Ward NS (2014) Cortical reorganization after stroke: how much and how functional? *The Neuroscientist* 20:56–70.

Haegens S, Nácher V, Luna R, Romo R, Jensen O (2011) α-oscillations in the monkey sensorimotor network influence discrimination performance by rhythmical inhibition of neuronal spiking. *Proceedings of the National Academy of Sciences* 108:19377–19382.

Hall TM, de Carvalho F, Jackson A (2014) A common structure underlies low-frequency cortical dynamics in movement, sleep, and sedation. *Neuron* 83:1185–1199.

Harrison TC, Ayling OG, Murphy TH (2012) Distinct cortical circuit mechanisms for complex forelimb movement and motor map topography. *Neuron* 74:397–409.

JNeurosci Accepted Manuscript

Hira R, Ohkubo F, Tanaka YR, Masamizu Y, Augustine GJ, Kasai H, Matsuzaki M (2013) In vivo optogenetic tracing of functional corticocortical connections between motor forelimb areas. *Frontiers in neural circuits* 7:55.

Hooks B, Hires SA, Zhang YX, Huber D, Petreanu L, Svoboda K, Shepherd GM (2011) Laminar analysis of excitatory local circuits in vibrissal motor and sensory cortical areas. *PLoS biology* 9:e1000572.

Isaacson JS, Scanziani M (2011) How inhibition shapes cortical activity. *Neuron* 72:231–243.

Isomura Y, Harukuni R, Takekawa T, Aizawa H, Fukai T (2009) Microcircuitry coordination of cortical motor information in self-initiation of voluntary movements. *Nature neuroscience* 12:1586–1593.

Jaenisch N, Liebmann L, Guenther M, Hübner CA, Frahm C, Witte OW (2016) Reduced tonic inhibition after stroke promotes motor performance and epileptic seizures. *Scientific reports* 6:26173.

Kargo WJ, Nitz DA (2004) Improvements in the signal-to-noise ratio of motor cortex cells distinguish early versus late phases of motor skill learning. *Journal of Neuroscience* 24:5560–5569.

Khanna P, Carmena JM (2017) Beta band oscillations in motor cortex reflect neural population signals that delay movement onset. *elife* 6:e24573.

Khanna P, Totten D, Novik L, Roberts J, Morecraft RJ, Ganguly K (2021) Low-frequency stimulation enhances ensemble co-firing and dexterity after stroke. *Cell* 184:912–930.

Le Van Quyen M, Foucher J, Lachaux JP, Rodriguez E, Lutz A, Martinerie J, Varela FJ (2001) Comparison of hilbert transform and wavelet methods for the analysis of neuronal synchrony. *Journal of neuroscience methods* 111:83–98.

Li Q, Ko H, Qian ZM, Yan LY, Chan DC, Arbuthnott G, Ke Y, Yung WH (2017) Refinement of learned skilled movement representation in motor cortex deep output layer. *Nature communications* 8:15834.

Longa EZ, Weinstein PR, Carlson S, Cummins R (1989) Reversible middle cerebral artery occlusion without craniectomy in rats. *stroke* 20:84–91.

JNeurosci Accepted Manuscript

Luck SJ (2014) *An introduction to the event-related potential technique* MIT press.

Maris E, Oostenveld R (2007) Nonparametric statistical testing of eeg-and meg-data. *Journal of neuroscience methods* 164:177–190.

Mimica B, Tombaz T, Battistin C, Fuglstad JG, Dunn BA, Whitlock JR (2023) Behavioral decomposition reveals rich encoding structure employed across neocortex in rats. *Nature Communications* 14:3947.

Mizuseki K, Sirota A, Pastalkova E, Buzsáki G (2009) Theta oscillations provide temporal windows for local circuit computation in the entorhinal-hippocampal loop. *Neuron* 64:267–280.

Murase N, Duque J, Mazzocchio R, Cohen LG (2004) Influence of interhemispheric interactions on motor function in chronic stroke. *Annals of Neurology: Official Journal of the American Neurological Association and the Child Neurology Society* 55:400–409.

Natraj N, Silversmith DB, Chang EF, Ganguly K (2022) Compartmentalized dynamics within a common multi-area mesoscale manifold represent a repertoire of human hand movements. *Neuron* 110:154–174.

Nawrot MP, Boucsein C, Molina VR, Riehle A, Aertsen A, Rotter S (2008) Measurement of variability dynamics in cortical spike trains. *Journal of neuroscience methods* 169:374–390.

Nudo RJ (2006) Mechanisms for recovery of motor function following cortical damage. *Current opinion in neurobiology* 16:638–644.

Peters AJ, Chen SX, Komiyama T (2014) Emergence of reproducible spatiotemporal activity during motor learning. *Nature* 510:263–267.

Ramanathan D, Conner JM, H. Tuszynski M (2006) A form of motor cortical plasticity that correlates with recovery of function after brain injury. *Proceedings of the National Academy of Sciences* 103:11370–11375.

Ramanathan DS, Gulati T, Ganguly K (2015) Sleep-dependent reactivation of ensembles in motor cortex promotes skill consolidation. *PLoS biology* 13:e1002263.

Ramanathan DS, Guo L, Gulati T, Davidson G, Hishinuma AK, Won SJ, Knight RT, Chang EF, Swanson RA, Ganguly K (2018) Low-frequency cortical activity is a neuromodulatory target that tracks recovery after stroke. *Nature medicine* 24:1257–1267.

JNeurosci Accepted Manuscript

Rehme AK, Grefkes C (2013) Cerebral network disorders after stroke: evidence from imaging-based connectivity analyses of active and resting brain states in humans. *The Journal of physiology* 591:17–31.

Riehle A, Wirtssohn S, Grün S, Brochier T (2013) Mapping the spatio-temporal structure of motor cortical lfp and spiking activities during reach-to-grasp movements. *Frontiers in neural circuits* 7:48.

Rogers DC, Campbell CA, Stretton JL, Mackay KB (1997) Correlation between motor impairment and infarct volume after permanent and transient middle cerebral artery occlusion in the rat. *Stroke* 28:2060–2066.

Rule ME, Vargas-Irwin C, Donoghue JP, Truccolo W (2015) Contribution of lfp dynamics to single-neuron spiking variability in motor cortex during movement execution. *Frontiers in systems neuroscience* 9:89.

Saikaley M, Pauli G, Sun H, Serra JR, Iruthayarajah J, Teasell R (2022) Network meta-analysis of non-conventional therapies for improving upper limb motor impairment poststroke. *Stroke* 53:3717–3727.

Saleh M, Reimer J, Penn R, Ojakangas CL, Hatsopoulos NG (2010) Fast and slow oscillations in human primary motor cortex predict oncoming behaviorally relevant cues. *Neuron* 65:461–471.

Schalk G, Kubanek J, Miller KJ, Anderson N, Leuthardt EC, Ojemann JG, Limbrick D, Moran D, Gerhardt LA, Wolpaw JR (2007) Decoding two-dimensional movement trajectories using electrocorticographic signals in humans. *Journal of neural engineering* 4:264.

Schönfeld LM, Dooley D, Jahanshahi A, Temel Y, Hendrix S (2017) Evaluating rodent motor functions: Which tests to choose? *Neuroscience & Biobehavioral Reviews* 83:298–312.

Tanji J, Okano K, Sato KC (1987) Relation of neurons in the nonprimary motor cortex to bilateral hand movement. *Nature* 327:618–620.

Tanji J, Okano K, Sato KC (1988) Neuronal activity in cortical motor areas related to ipsilateral, contralateral, and bilateral digit movements of the monkey. *Journal of neurophysiology* 60:325–343.

JNeurosci Accepted Manuscript

Taube JS (2010) Interspike interval analyses reveal irregular firing patterns at short, but not long, intervals in rat head direction cells. *Journal of Neurophysiology* 104:1635–1648.

Touvykine B, Elgbeili G, Quessy S, Dancause N (2020) Interhemispheric modulations of motor outputs by the rostral and caudal forelimb areas in rats. *Journal of neurophysiology* 123:1355–1368.

VanRullen R (2016) Perceptual cycles. *Trends in cognitive sciences* 20:723–735.

Vinck M, Van Wingerden M, Womelsdorf T, Fries P, Pennartz CM (2010) The pairwise phase consistency: a bias-free measure of rhythmic neuronal synchronization. *Neuroimage* 51:112–122.

Voloh B, Oemisch M, Womelsdorf T (2020) Phase of firing coding of learning variables across the fronto-striatal network during feature-based learning. *Nature communications* 11:4669.

Wang HL, Kuo YT, Lo YC, Kuo CH, Chen BW, Wang CF, Wu ZY, Lee CE, Yang SH, Lin SH et al. (2023) Enhancing prediction of forelimb movement trajectory through a calibrating-feedback paradigm incorporating rat primary motor and agranular cortical ensemble activity in the goal-directed reaching task. *International journal of neural systems* 33:2350051.

Ward N, Brown M, Thompson A, Frackowiak R (2003) Neural correlates of motor recovery after stroke: a longitudinal fmri study. *Brain* 126:2476–2496.

Yang W, Kanodia H, Arber S (2023) Structural and functional map for forelimb movement phases between cortex and medulla. *Cell* 186:162–177.

York GK (2002) Motor testing in neurology: an historical overview. *Seminars in Neurology* 22:367–374.

Yu Z, Guindani M, Grieco SF, Chen L, Holmes TC, Xu X (2022) Beyond t test and anova: applications of mixed-effects models for more rigorous statistical analysis in neuroscience research. *Neuron* 110:21–35.

Zheng J, Schjetnan AG, Yebra M, Gomes BA, Mosher CP, Kalia SK, Valiante TA, Mamelak AN, Kreiman G, Rutishauser U (2022) Neurons detect cognitive boundaries to structure episodic memories in humans. *Nature neuroscience* 25:358–368.

JNeurosci Accepted Manuscript

JNeurosci Accepted Manuscript

1 Figures

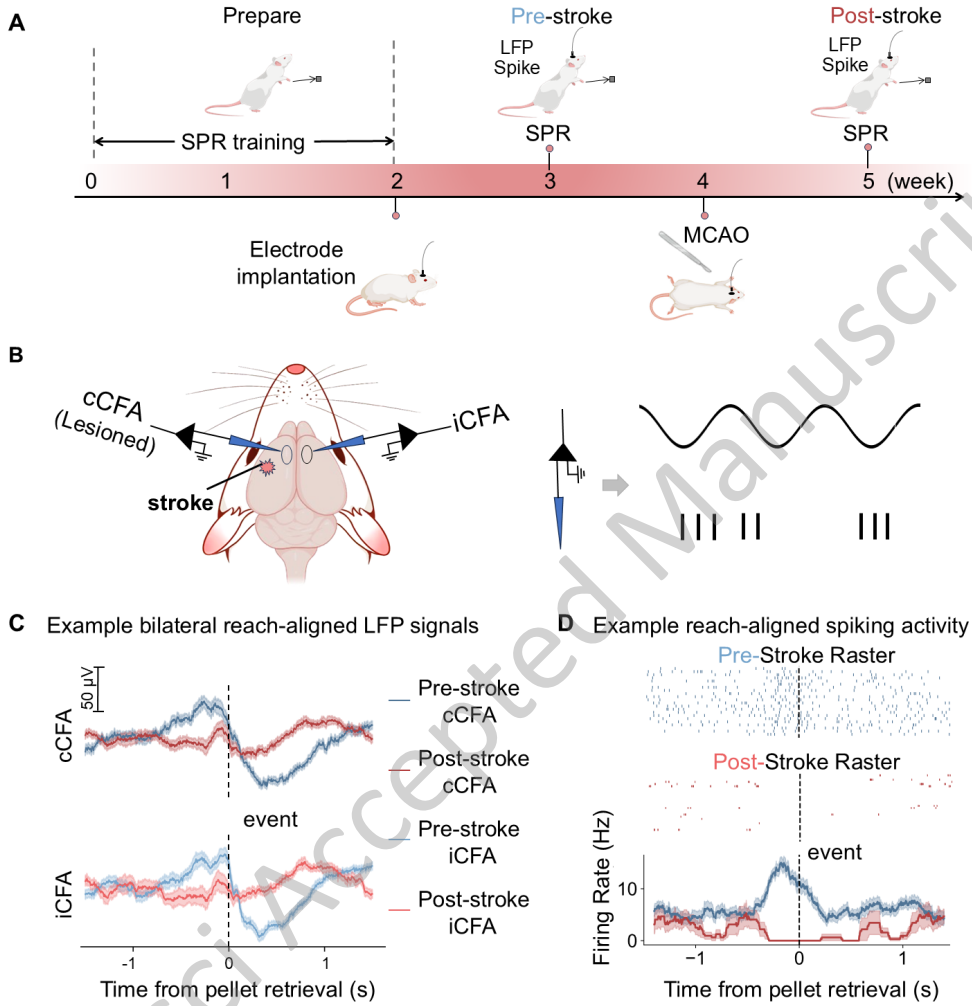


Figure 1: Experimental framework and examples of movement-related population and spiking activity before and early after stroke. (A) Experimental timeline illustrating SPR training, electrode implantation, MCAO induction, and neural recordings during the SPR task one week before (pre-stroke) and one week after (early post-stroke) MCAO. (B) Schematic of bilateral neural recordings from cCFA (lesioned) and iCFA. (C) Trial-averaged movement-related LFP waveforms (±SEM) across trials from one rat, aligned to pellet retrieval, recorded from cCFA (lesioned) and iCFA before and early after stroke. (D) Representative movement-related spike raster plots and corresponding firing rate of a neuron from the same rat, aligned to pellet retrieval, across trials before and early after stroke.

JNeurosci Accepted Manuscript

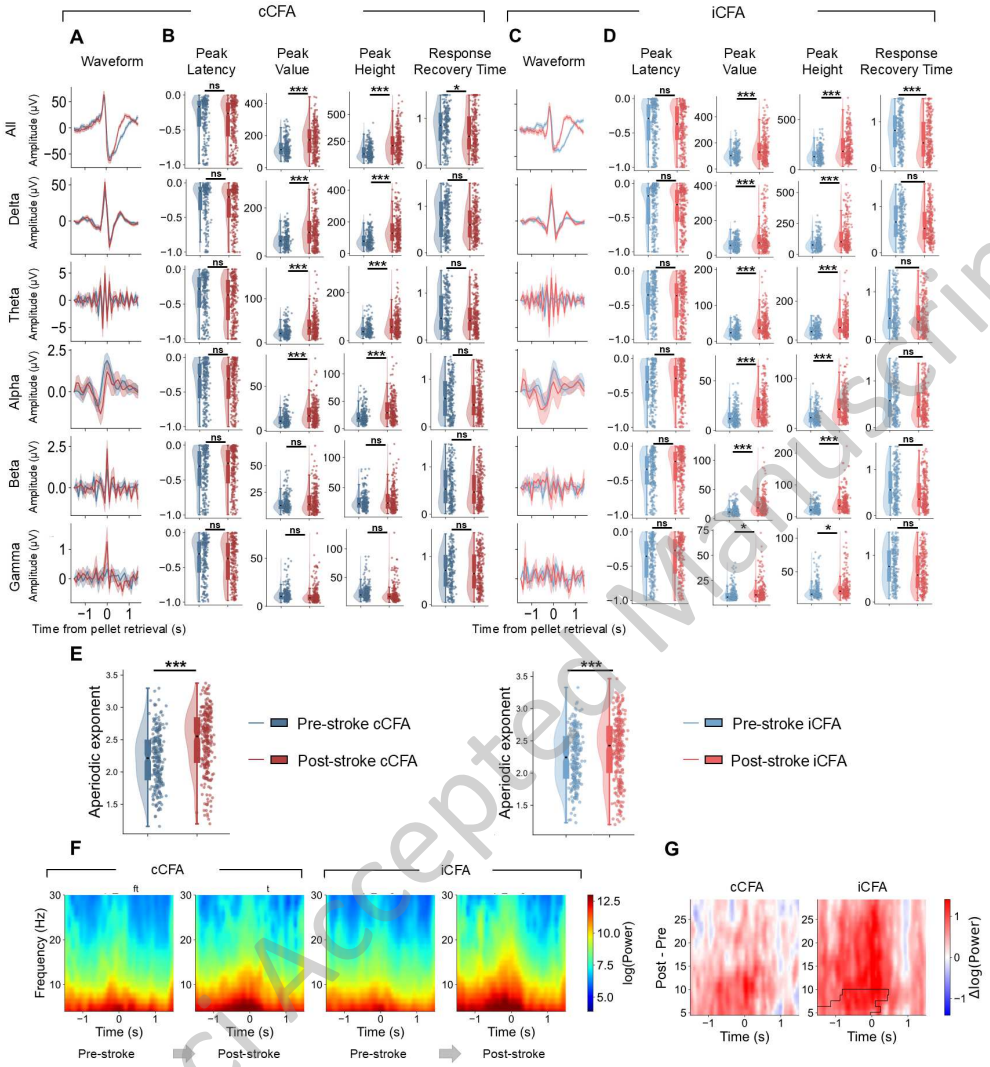


Figure 2: Preserved movement-related response latency with reorganized spectral and recovery dynamics. (A-B) Movement-related LFP waveforms (A) and corresponding peak metrics (B) recorded from the cCFA during the SPR task, shown separately for pre-stroke (blue) and early post-stroke (red) conditions. Peak value, peak latency, peak height, and response recovery time were quantified for raw LFP signals ("All") and for band-pass-filtered LFPs in five canonical frequency bands (delta, theta, alpha, beta, and gamma). (C-D) Same analyses as in A and B for the iCFA. (E) Estimated aperiodic exponent of the LFP power spectrum (log-log domain) before and early after stroke, showing significant steepening in both hemispheres. (F) Time-frequency representations of LFP power (4–30 Hz) aligned to pellet retrieval in the cCFA and iCFA before and early after stroke. Color indicates log-transformed power averaged across epochs. (G) Post-pre difference in time-frequency power (Δlog power). Black contours indicate clusters with significant differences identified using cluster-based permutation tests. Data are shown as raincloud plots, combining individual observations (scatter), box plots (median and interquartile range), and half-violin density distributions. Statistical significance is indicated as ns $p > 0.05$; $**$ $p < 0.01$; $***$ $p < 0.001$.

JNeurosci Accepted Manuscript

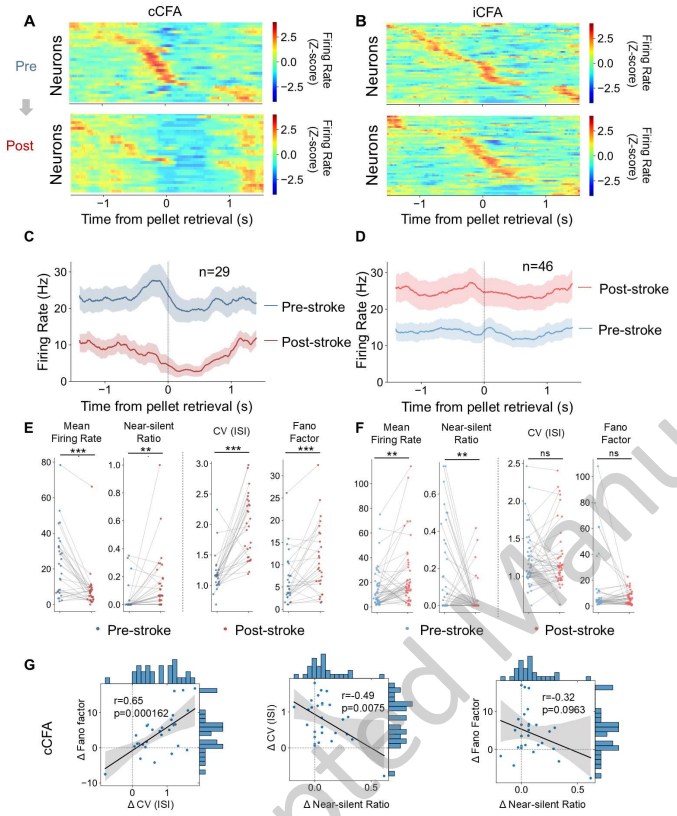


Figure 3: Movement-related spiking dynamics show reorganized neuronal recruitment and variability structure across hemispheres following stroke. (A-B) Movement-related PETH heatmaps of firing rates (z-scored) for neurons at the population level in cCFA (A) and iCFA (B) before (Pre) and after (Post) perturbation. Each row represents an individual unit, independently sorted within each condition by movement-related peak firing rate. Color indicates z-scored firing rate. (C-D) Population-averaged firing rate time courses aligned to pellet retrieval (dashed line) for the cCFA (C; n=29 units) and iCFA (D; n=46 units), shown for pre-stroke (blue) and early post-stroke (red) conditions (mean ± SEM). (E-F) Paired comparisons of unit-level spike metrics during the single-pellet retrieval (SPR) task for neurons in the cCFA (E) and iCFA (F), including mean firing rate, near-silent ratio, coefficient of variation of inter-spike intervals (CV(ISI)), and Fano factor, measured before (pre-stroke) and after (early post-stroke) perturbation (paired differences computed as pre-post). Each dot represents one unit, and lines connect paired measurements from the same unit across conditions. Two-sided paired t-tests with FDR corrected for multiple comparison were used for statistical comparisons (mean firing rate: $t = 5.94$, $p < 0.001$; near-silent ratio: $t = -3.25$, $p < 0.01$; CV(ISI) within a trial: $t = -3.85$, $p < 0.001$; Fano factor across trials: $t = -7.36$, $p < 0.001$). Two-sided paired t-tests were used for statistical comparisons (mean firing rate: $t = -3.48$, $p < 0.01$; near-silent ratio: $t = 2.95$, $p < 0.01$; CV(ISI): $t = 1.93$, $p > 0.05$; Fano factor: $t = -0.11$, $p > 0.05$). (G) Variability and recruitment coupling in the cCFA. Unit-wise relationships between post–pre changes (Δ) in spike variability and recruitment metrics, including the relationship between ΔCV(ISI) and ΔFano factor, between Δnear-silent ratio and ΔCV(ISI), and between Δnear-silent ratio and ΔFano factor. Each point represents one unit. Solid lines indicate linear regression fits with 95% confidence intervals; marginal histograms show distributions of each variable; correlation statistics report Pearson's r. Data in (E–F) are shown as paired dot plots with connecting lines between pre- and early post-stroke measurements for each unit. Data in (G) are shown as joint scatter plots with marginal histograms. Statistical significance is indicated as ns ($p > 0.05$); * ($p < 0.05$); ** ($p < 0.01$); *** ($p < 0.001$).

JNeurosci Accepted Manuscript

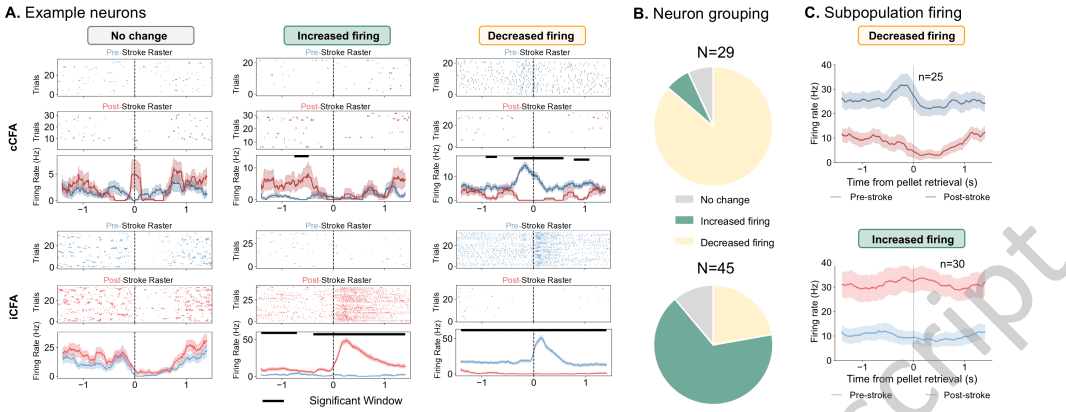


Figure 4: Single-unit subpopulations showing early post-stroke increases or decreases in cCFA and iCFA. (A) Representative single-unit examples illustrating three response patterns observed early after stroke: increased firing, decreased firing, and no change. Examples are shown for cCFA (top) and iCFA (bottom). For each unit, pre-stroke and early post-stroke spike rasters are shown on separate rows, followed by the movement-related mean firing rate trajectories (mean ± SEM). Black bars indicate significant temporal clusters identified by cluster permutation tests. (B) Based on the predominant sign of the post-pre firing-rate difference within significant temporal clusters (see Methods), neurons were grouped into increased-firing, decreased-firing, or no-change categories. Pie charts summarize the proportion of units in each category (cCFA: N=29; iCFA: N=45), highlighting the dominant direction of change in each hemisphere. (C) Population-averaged firing rate time courses aligned to pellet retrieval (dashed line) for contralateral decreased-firing units (n=25) and ipsilateral increased-firing units (n=30), shown for pre-stroke (blue) and early post-stroke (red) conditions (mean ± SEM). One ipsilateral unit with no detectable early post-stroke spikes was excluded from the temporal cluster-based subpopulation classification; therefore, the ipsilateral sample size was (N=45) in this analysis.

JNeurosci Accepted Manuscript

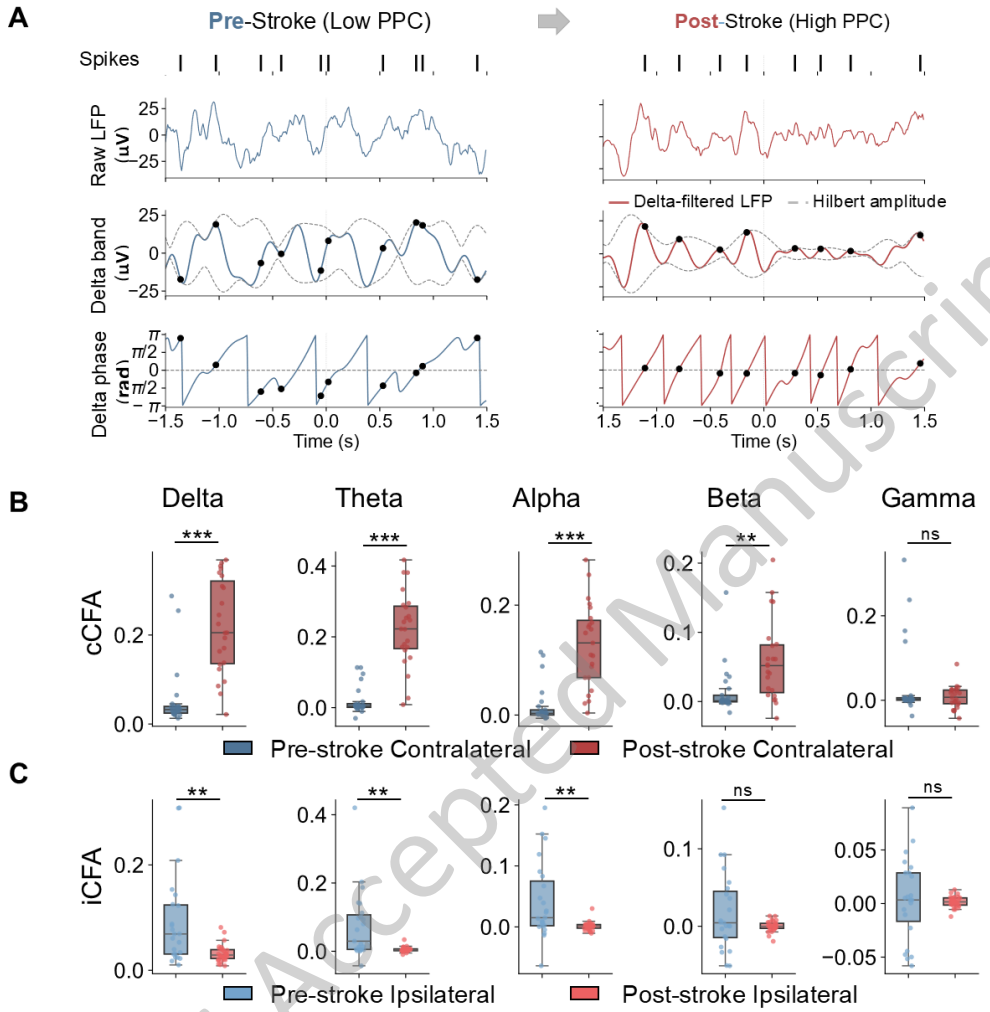


Figure 5: Stroke alters spike–LFP phase consistency in opposite directions across the bilateral caudal forelimb areas (CFA). A, Schematic of the PPC analysis pipeline, illustrated using examples with low (left) and high (right) PPC. From top to bottom, the pipeline shows the raw LFP trace, the LFP band-pass filtered in the delta band together with its amplitude envelope, and the instantaneous delta phase. Black dots mark spike times. Spike phases sampled from the instantaneous phase trace are dispersed in the low-PPC example but cluster around a similar phase in the high-PPC example. (B–C), Pairwise phase consistency (PPC) of spike–LFP phase relationships in the cCFA (B) and iCFA (C) across canonical frequency bands (delta–gamma), shown for pre-stroke (blue) and early post-stroke (red) conditions. cCFA is shown in dark blue (pre-stroke) and dark red (early post-stroke), whereas iCFA is shown in light blue (pre-stroke) and light red (early post-stroke). PPC quantifies the consistency of spike timing relative to the ongoing LFP phase across trials, with higher values indicating more reliable spike–phase alignment. Box plots indicate the median (center line) and interquartile range (box), with individual points representing single cells. Statistical significance was assessed using *t*-tests with Benjamini–Hochberg false discovery rate (FDR-BH) correction.

JNeurosci Accepted Manuscript

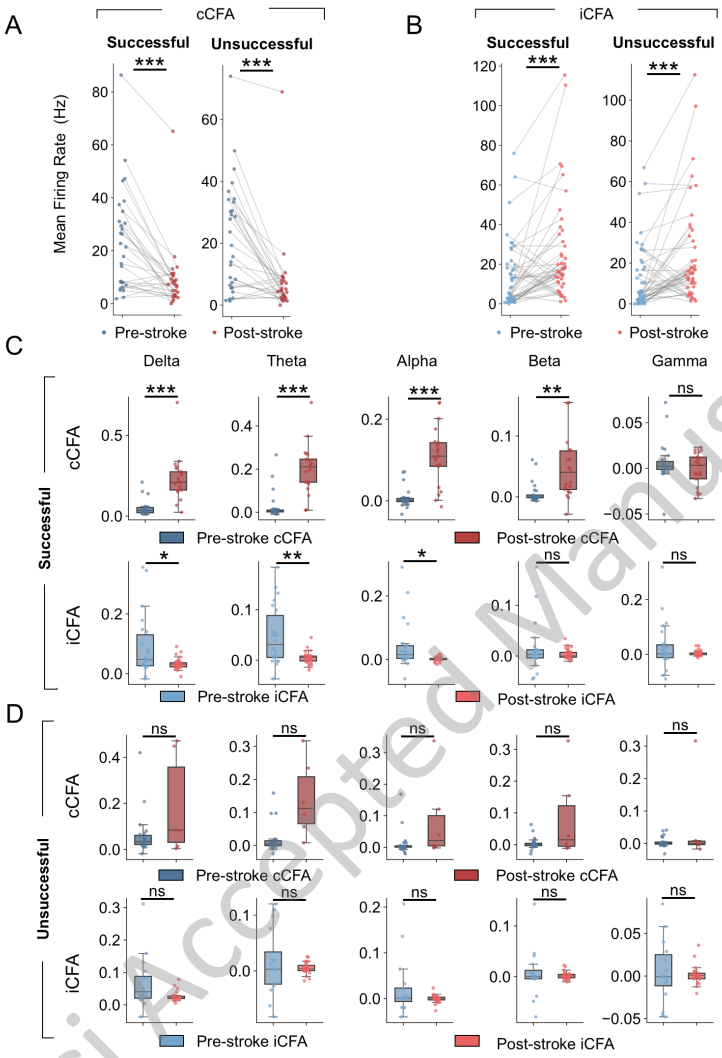


Figure 6: Firing rate and pairwise phase consistency (PPC) during successful and unsuccessful single-pellet retrieval (SPR) trials before and early after stroke. (A–B) Unit-level mean firing rates in the cCFA (A) and iCFA (B). In each panel, the left plot shows successful pellet-grasp trials and the right plot shows unsuccessful pellet-grasp trials. Each dot represents one unit, and lines connect measurements from the same unit across the pre-stroke and early post-stroke conditions. Paired differences were calculated as pre-stroke minus early post-stroke. Two-sided paired t-tests showed significant changes in firing rate for contralateral successful trials ($t = 5.422$, $p < 0.001$), contralateral unsuccessful trials ($t = 5.345$, $p < 0.001$), ipsilateral successful trials ($t = -3.640$, $p < 0.001$), and ipsilateral unsuccessful trials ($t = -3.525$, $p < 0.001$). (C–D) PPC of spike–LFP phase relationships across canonical frequency bands from delta to gamma during successful trials (C) and unsuccessful trials (D). In each panel, the cCFA is shown in the upper row and the iCFA in the lower row. Pre-stroke and early post-stroke conditions are shown in blue and red, respectively; darker colors indicate the cCFA and lighter colors indicate the iCFA. Higher PPC values indicate more consistent spike timing relative to the ongoing LFP phase. Box plots show the median and interquartile range, and individual points represent single units. Statistical significance was assessed using two-sided t-tests.

JNeurosci Accepted Manuscript

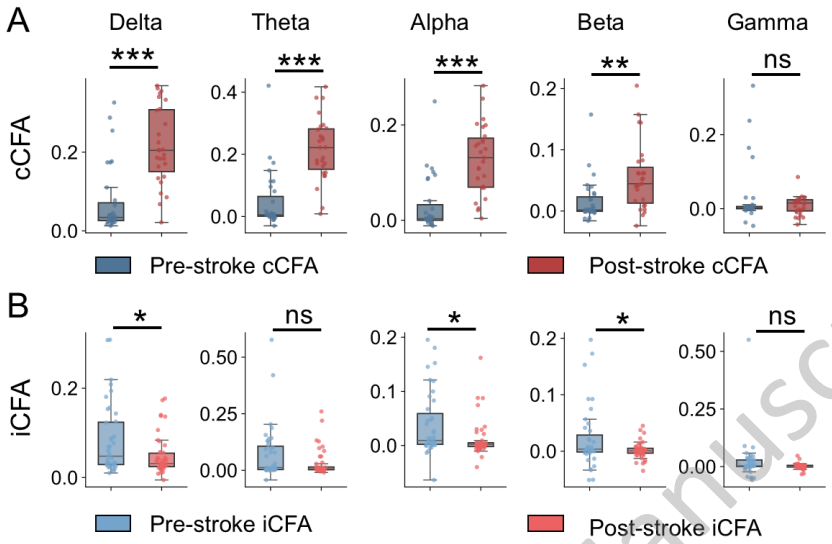


Figure 7: Pairwise phase consistency across the full unit population before and after stroke. (A–B) Pairwise phase consistency (PPC) of spike–LFP phase relationships across all eligible units in the contralateral (A) and ipsilateral (B) CFA across canonical frequency bands (delta–gamma), shown for pre-stroke and post-stroke conditions. Contralateral CFA is shown in dark blue (pre-stroke) and dark red (post-stroke), whereas ipsilateral CFA is shown in light blue (pre-stroke) and light red (post-stroke). PPC quantifies the consistency of spike timing relative to the ongoing LFP phase, with higher values indicating more reliable spike–phase alignment. Box plots indicate the median (center line) and interquartile range (box), with individual points representing single units. Statistical significance was assessed using t-tests with Benjamini–Hochberg false discovery rate (FDR-BH) correction. Statistical significance is indicated as ns ($p_{\mathrm{FDR}} > 0.05$); * ($p_{\mathrm{FDR}} < 0.05$); ** ($p_{\mathrm{FDR}} < 0.01$); *** ($p_{\mathrm{FDR}} < 0.001$).

JNeurosci Accepted Manuscript

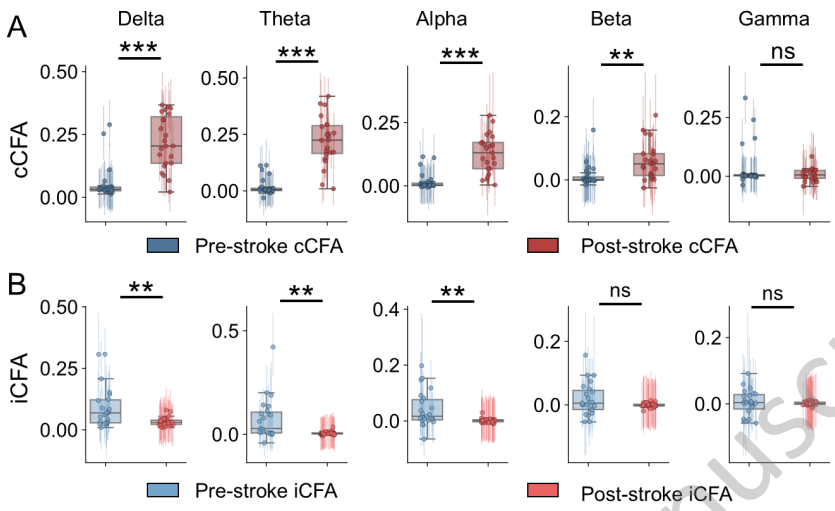


Figure 8: Spike-count-matched pairwise phase consistency before and early after stroke. (A–B) Spike–LFP phase consistency in the cCFA (A) and iCFA (B) after controlling the number of spikes contributing from each trial. For each eligible trial, five spike-associated phases were randomly sampled without replacement, and trial-wise PPC was calculated from the sampled phases. Trial-wise PPC values were then averaged across valid trials to obtain one PPC estimate for each resampling iteration. This random subsampling procedure was repeated 1,000 times for each unit. Each point represents the mean PPC across the 1,000 resampling iterations for an individual unit, and vertical lines indicate the corresponding 2.5th–97.5th percentile range of the resampling distribution. Pre-stroke and early post-stroke conditions are shown in blue and red, respectively. Statistical comparisons were performed on the unit-level mean PPC values using two-sided Welch's t-tests with Benjamini–Hochberg FDR correction across the 10 hemisphere-by-frequency-band comparisons. Statistical significance is indicated as ns ($p_{\mathrm{FDR}} > 0.05$), * ($p_{\mathrm{FDR}} < 0.05$), ** ($p_{\mathrm{FDR}} < 0.01$), and *** ($p_{\mathrm{FDR}} < 0.001$).

2 Tables

JNeurosci Accepted Manuscript

Table 1: Number of analyzed trials before and early after stroke for each rat.

Animal	**Pre-stroke trials**	**Early post-stroke trials**
1	26	33
2	35	32
3	22	32
4	37	18
5	31	31
6	33	21
7	31	34
8	31	32

JNeurosci Accepted Manuscript